

## Multicomponent reactive transport in discrete fractures II: Infiltration of hyperalkaline groundwater at Maqarin, Jordan, a natural analogue site

C.I. Steefel<sup>a,\*</sup>, P.C. Lichtner<sup>b,1</sup>

<sup>a</sup>Department of Geosciences, University of South Florida, Tampa, FL 33620, USA

<sup>b</sup>Center for Nuclear Waste Regulatory Analyses, Southwest Research Institute, San Antonio, TX 78238-5166, USA

Received 19 June 1997; received in revised form 29 May 1998; accepted 29 May 1998

### Abstract

A numerical multicomponent reactive transport model described fully in Steefel and Lichtner (1998)[Steefel, C.I., Lichtner, P.C., 1998. Multicomponent reactive transport in discrete fractures, I. Controls on reaction front geometry. *J. Hydrol.* (in press)] is used to simulate the infiltration of hyperalkaline groundwater along discrete fractures at Maqarin, Jordan, a site considered as a natural analogue to cement-bearing nuclear waste repositories. In the Eastern Springs area at Maqarin, two prominent sets of sub-parallel fractures trending NW–SE are approximately perpendicular to the local water table contours, with the slope of the water table indicating north-westward flow. Extensive mineralogic investigations [Alexander W.R. (Ed.), 1992. A natural analogue study of cement-buffered, hyperalkaline groundwaters and their interaction with a sedimentary host rock. NAGRA Technical Report (NTB 91-10), Wettingen, Switzerland; Milodowski, A.E., Hyslop, E.K., Pearce, J.M., Wetton, P.D., Kemp, S.J., Longworth, G., Hodginson, E., and Hughes, C.R., 1998, Mineralogy and geochemistry of the western springs area. In: Smellie, J.A.T. (ed.), 1998: Maqarin Natural Analogue Study: Phase III. SKB Technical Report TR 98-04, Stockholm, Sweden] indicate that the width of intense rock alteration zone bordering the fractures changes from about 4 mm at one locality (the M1 sampling site) to approximately 1 mm 100 m to the north-west in the flow direction (the M2 site), suggesting a lessening of alteration intensity in that direction. Using this information, the dimensionless parameter  $\delta\nu/\phi D'$  ( $\phi$  = porosity,  $D'$  = effective diffusion coefficient in rock matrix,  $\delta$  = fracture aperture, and  $\nu$  = fluid velocity in the fracture) and measurements of the local hydraulic head gradient and effective diffusion coefficient in the rock matrix, a mean fracture aperture of 0.194 mm is calculated assuming the cubic law applies. This information, in combination with measured groundwater compositions at the Maqarin site, is used as input for numerical simulations of the hyperalkaline groundwater infiltration along fractures. The width of the alteration zones in the rock matrix bordering fractures is also used to constrain mineral dissolution rates in the field.

The simulations predict that ettringite [ $\text{Ca}_6\text{Al}_2(\text{SO}_4)_3(\text{OH})_{12}\cdot 26\text{H}_2\text{O}$ ] with lesser amounts of hillebrandite and tobermorite (hydrated calcium silicates or CSH phases) will be the dominant alteration products forming at the expense of the primary silicates in the rock matrix and fracture, in agreement with observations at the Maqarin site. The simulations also come close to matching the pH of water samples collected along fractures at the M1 and M2 sites, with a fracture aperture of 0.22 mm giving the closest match with the pH data (within 13% of the value indicated by the rock matrix alteration widths). The simulations suggest two possible scenarios for the time evolution of the fracture–rock matrix system. Where rate constants for secondary mineral precipitation reactions are the same in both the rock matrix and fracture, the rock matrix tends to become

\* Corresponding author. Fax: +1- 813-9742654; e-mail: steefel@margaux.cas.usf.edu

<sup>1</sup> Present address: Los Alamos National Laboratory, P.O. Box 1663, Mail Stop C305, EES-5, Los Alamos, NM 87545.

completely cemented before the fracture. This results in a downstream migration of the hyperalkaline plume. In contrast, if rates are as little as one order of magnitude higher in the fracture than in the rock matrix, it is possible to seal the fracture first, thus causing the mineral zones to collapse upstream as a result of the reduction in fracture permeability. Sealing of fractures is observed at Maqarin and the simulations predict a mineral paragenesis in the fracture resulting from this scenario which is broadly compatible with field observations. © 1998 Elsevier Science B.V. All rights reserved.

*Keywords:* Multicomponent reactive transport; Discrete fractures; Hyperalkaline groundwater; Wall-rock alteration

---

## 1. Introduction

The intention of many nations to dispose of radioactive wastes in low-permeability formations has led to an increased interest in the behavior of contaminants in fractures. In many of these cases, the permeability represented by the fractures is orders of magnitude larger than the permeability of the rock matrix, whereas the bulk rock fracture porosity is much smaller than the matrix porosity. A growing body of work is devoted to understanding the physics of flow and transport in discrete fracture systems (Neretnieks, 1980; Tang et al., 1981; Neretnieks et al., 1982; Moreno et al., 1985; Skagius and Neretnieks, 1986; Moreno et al., 1988; Tsang and Tsang, 1989; Moreno et al., 1990; Cacas et al., 1991; Cvetkovic, 1991; Dykhuizen, 1992; Thoma et al., 1992; Maloszewski and Zuber, 1993; Moreno and Neretnieks, 1993; Nordqvist et al., 1996; Therrien and Sudicky, 1996; Odling and Roden, 1997; Park et al., 1997; Vandergraaf et al., 1997). A much smaller amount of research, however, has focused on the coupling of multicomponent chemical reactions and transport in such systems (Novak and Sevougian, 1992; Steefel and Lichtner, 1994; Novak, 1996; Steefel and Lichtner, 1998).

While flow velocities in fractures are often relatively high, diffusion into the rock matrix can significantly reduce the effective solute velocities in the fracture and retard the rate of contaminant migration (Neretnieks, 1980). Even in the absence of any kind of chemical reaction, the diffusive loss of solutes into the rock matrix bordering fractures may be significant, justifying the need to consider a model incorporating fracture–matrix interaction for transport in fractured media. Matrix diffusion will be even more important in the case where chemical reactions affect the mobility of contaminants, since the rock matrix provides additional sorption and buffering capacity

(Neretnieks, 1980; Tang et al., 1981; Steefel and Lichtner, 1994; Novak, 1996).

An important issue that arises in assessing the likely performance of nuclear waste repositories is whether the physical and chemical properties of the fractured host rocks will remain constant for the life of the repository (McKinley and Alexander, 1993; Steefel and Lichtner, 1994; Smellie et al., 1997). Because nuclear waste repositories need to function over long periods of times (hundreds to tens of thousands of years), reaction-induced modifications of the physical and chemical properties of the near-field host rock may be important. In certain cases, significant modifications to the hydrologic and chemical character of the near-field rocks may occur on the time scale of hundreds of years or less. Using one-dimensional reaction–diffusion calculations, Steefel and Lichtner (1994), for example, suggested that the porosity of a rock matrix with a marl composition such as would be found in the near-field surrounding the proposed Swiss low-level waste repository could be substantially modified within as little as tens of years. The greatest uncertainty in this estimate appears to be the magnitude of the reacting surface area of minerals used in the calculations. Steefel and Lichtner (1994) pointed to several possible effects, including a porosity increase or decrease in the rock matrix and fracture. A porosity decrease in the rock matrix could affect effective solute velocities in the fracture by (1) decreasing the effective diffusion coefficients for solutes in the matrix, thus reducing the ‘diffusive loss’ to the matrix, and (2) by reducing the amount of reactive surface area on minerals available for both sorption and dissolution (and possibly precipitation) reactions.

A related issue in the design of a nuclear waste repository is how the materials used in its construction may affect performance. Much of the attention in this regard has focused on the use of large amounts of

cement in repositories, since groundwaters reacting with the cement may attain very high pH values (Reardon, 1992). In terms of the performance assessment of the repository, the primary concern is that the groundwaters which have reacted with cement will be very far from equilibrium with respect to the near-field repository host rocks, thus causing a number of reactions to take place which could alter the properties of the near-field rocks over relatively short periods of time.

The possible change in the hydrologic and chemical properties of the repository near-field may be one of the prime reasons why it is difficult to predict repository performance over the long periods of time that they are expected to function. While realistic field-scale experiments are an essential part of the performance assessment analysis, the length of time that they can be carried out is limited. Workers have turned, therefore, to natural analogue sites (e.g. McKinley and Alexander, 1992; McKinley and Alexander, 1993) where one or more of the processes or conditions expected at the repository site has been operating for substantial lengths of time. One such site which is being actively investigated is located at Maqarin, Jordan where the dissolution of naturally-occurring portlandite (the principal component of cement) has led to high pH groundwater infiltrating the local rock along fractures (Alexander, 1992; Alexander et al., 1998). Extensive mineralogic, hydrogeochemical, and isotopic investigations of the site have documented a complex suite of alteration products resulting from the hyperalkaline groundwater infiltration. Despite the widespread occurrence of alteration effects and even completely sealed fractures, high pH groundwater can be sampled at the site (Waber et al., 1998), indicating the system is still active.

In this paper, we use the numerical multicomponent reactive transport model and the results on reaction front geometries described in Steefel and Lichtner (1998) to interpret the mineralogic alteration effects and the hydrogeochemistry of the Eastern Springs area at Maqarin, Jordan. Of particular interest is whether the mineralogic alteration observed in and along fractures at Maqarin is compatible with the observed hydrogeochemistry of springs at the site. In addition, we are interested in obtaining a first order estimate of the rate of fracture permeability

and rock matrix porosity modification, assuming that we can match most or all of the significant observations at the site. Finally, we wish to see whether a fully coupled dynamic model of the kind used here can offer any insight into the complex sequence of mineralogic events (i.e. the mineral paragenesis) at Maqarin.

## 2. Physical system

Consider a thin nondeformable fracture developed within a saturated porous rock matrix with a significantly lower permeability compared with the fracture such that flow within the rock matrix is negligible (Fig. 1). Solute transport within the rock matrix, therefore, is via molecular diffusion only. Steady-state flow in the fracture is assumed. The fracture is assumed to have a constant aperture and smooth parallel walls initially. In addition, we assume in all cases that the width of the fracture is much smaller than its length and that transverse diffusion and dispersion within the fracture cause complete mixing across the fracture width. The rock matrix is assumed to have initially homogeneous physical and chemical properties. Finally, a constant concentration boundary condition is assumed to exist at the inlet to the fracture, with a hyperalkaline composition acquired by reaction with portlandite occurrences in the metamorphosed rock at Maqarin. Assuming that the rock consists of a set of equally spaced, parallel fractures, symmetry requires a zero flux condition midway between fractures.

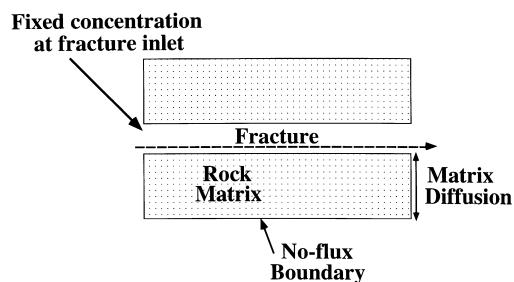


Fig. 1. Schematic representation of the explicit fracture model showing flow along a fracture with simultaneous diffusion into a rock matrix with low permeability. In the simulations, a fixed concentration is assumed at the fracture inlet.

### 3. Governing equations

#### 3.1. Formulation for discrete fractures

The mathematical formulation for multicomponent reaction in discrete fractures is described in detail in Steefel and Lichtner (1998). Briefly, the differential equations describing the conservation of solute mass in a single fracture can be written as

$$\frac{\partial C_j^f}{\partial t} = -v \frac{\partial C_j^f}{\partial z} + D \frac{\partial^2 C_j^f}{\partial z^2} - \sum_{s=1}^{N_s} \nu_{js} r_s + \frac{\phi D'}{\delta} \frac{\partial C_j^m}{\partial x} \Big|_{x=\delta},$$

( $j=1, \dots, N_c$ ) (1)

and for the rock matrix as

$$\frac{\partial}{\partial t} [\phi C_j^m] = \frac{\partial}{\partial x} \left[ \phi D' \frac{\partial C_j^m}{\partial x} \right] + \frac{\partial}{\partial z} \left[ \phi D' \frac{\partial C_j^m}{\partial z} \right] - \sum_{s=1}^{N_s} \nu_{js} r_s$$

(2)

where

$z$	coordinate along the fracture, L
$x$	coordinate perpendicular to fracture, L
$t$	time, T
$v$	groundwater velocity in the fracture, L/T
$C_j^f$	total dissolved concentration of $j$ th component in fracture, M/L <sup>3</sup>
$C_j^m$	total dissolved concentration of $j$ th component in rock matrix, M/L <sup>3</sup>
$\phi$	rock matrix porosity, dimensionless
$N_s$	number of reacting minerals in the system
$N_c$	number of independent chemical components in the system
$\nu_{js}$	stoichiometric reaction coefficient
$r_s$	reaction rate of mineral $m$ , M/L <sup>3</sup> T
$\tau$	tortuosity, dimensionless
$D'$	effective diffusion coefficient in the rock matrix ( $D' = \tau D_w$ ), M <sup>2</sup> /T
$D_w$	diffusion coefficient in water, M <sup>2</sup> /T
$D$	dispersion coefficient, M <sup>2</sup> /T
$2\delta$	fracture aperture, L

For a fuller discussion of the governing equations and associated parameters, see Steefel and Lichtner (1998).

#### 3.2. Fracture permeability and flow

We assume that fracture permeability is described by the ‘cubic law’ which states that rate of fluid flow

across a section of the fracture is proportional to the applied pressure gradient and the cube of fracture aperture (e.g. Snow, 1968; Phillips, 1991). The permeability for a set of parallel fractures with smooth walls is given by (Snow, 1968)

$$\kappa = \frac{\phi_f b^2}{12} = \frac{nb^3}{12} \quad (3)$$

where  $n$  is the number of fractures per unit distance across the rock (L<sup>-1</sup>),  $b$  is the fracture aperture ( $b = 2\delta$ ), and the fracture porosity,  $\phi_f$ , is related to the fracture density and aperture by the expression

$$\phi_f = nb \quad (4)$$

For practical purposes, the cubic law is assumed to hold over the length of a numerical grid cell along the fracture, allowing for the possibility that the fracture apertures evolve with time.

The Darcian flux in a unit volume of porous medium is given by

$$u = -\frac{\rho g \kappa}{\mu} \frac{\partial h}{\partial z} \quad (5)$$

where  $\mu$  is the fluid viscosity,  $\rho$  is the fluid density,  $g$  is the gravitational constant, and  $\partial h/\partial z$  is the gradient in hydraulic head in the fracture plane (de Marsily, 1986). Since the mean flow velocity  $v$  is related to the Darcian flux by

$$v = \frac{u}{\phi} = \frac{u}{nb} \quad (6)$$

the mean flow velocity can be written as

$$v = -\frac{\rho g b^2}{12\mu} \frac{\partial h}{\partial z} \quad (7)$$

#### 3.3. Kinetic formulation for mineral dissolution and precipitation

We use a kinetic rate law based on the assumption that attachment and detachment of ions from mineral surfaces is the rate-limiting step (i.e. a surface reaction-controlled rate law). The strong pH-dependence of the mineral dissolution reactions far from equilibrium is incorporated by including parallel reactions which are summed to give the overall rate law for a particular mineral (Steefel and Lichtner, 1998). The

rate law takes the form

$$r_s = -A_s \left\{ \sum_{l=1}^{N_{rs}} k_{ls} \left( \prod_{i=1}^{N_c + N_x} a_i^{p_{il}^s} \right) \right\} \left[ 1 - \frac{Q_s}{K_s} \right] \quad (8)$$

where  $k_{ls}$  is the far from equilibrium dissolution rate constant for the  $l$ th parallel reaction,  $p_{il}^s$  is the order of the  $l$ th parallel reaction,  $N_{rs}$  is the number of parallel reactions corresponding to the  $s$ th mineral,  $Q_s$  is the ion activity product,  $K_s$  is the equilibrium constant, and  $A_s$  refers to the surface area of individual minerals in the rock matrix or fracture. We have assumed here that the same dependence of the rate on the mineral saturation state applies for all of the various parallel reactions, although this need not be done.

In the simulations presented here, precipitation of minerals with high molar volumes locally cause the porosity to  $\rightarrow 0$ . We use the following expression to compute mineral surface areas as a function of the decreasing porosity

$$A_s(t) = A_s^o \left( \frac{\phi(t)}{\phi_o} \right)^{2/3} \quad (9)$$

where  $A_s^o$  and  $\phi_o$  refer to the initial surface area and initial porosity, respectively.

### 3.4. Mineral alteration equations

The mineral alteration equations for both fractures and the rock matrix have the form

$$\frac{\partial \phi_s}{\partial t} = \bar{V}_s r_s \quad (10)$$

where  $\bar{V}_s$  refers to the mineral molar volume and  $\phi_s$  refers to the mineral volume fractions. The porosity can be calculated directly from Eq. (10) (assuming no other processes result in a change in porosity) since

$$\phi = 1 - \sum_{s=1}^{N_s} \phi_s \quad (11)$$

The rate of change of the fracture aperture half-width can be related to the rate of change of the mineral volume fractions in the fracture by applying Eq. (10) to the fracture yielding

$$\frac{\partial \delta}{\partial t} = -\delta \sum_{s=1}^{N_s} \frac{\partial \phi_s^f}{\partial t} = -\delta \sum_{s=1}^{N_s} \bar{V}_s r_s \quad (12)$$

where  $\phi_s^f$  refers to the mineral volume fractions in the fracture. In finite difference form, this equation becomes

$$\delta(z, t + \Delta t) = \delta(z, t) \left( 1 - \Delta t \sum_s \bar{V}_s r_s \right) \quad (13)$$

This equation is used to update the fracture aperture as a function of time and space in the simulations.

## 4. Numerical solution method

The governing partial differential equations are solved with a slightly modified version of the code GIMRT (Steefel and Yabusaki, 1996) which uses a global implicit or one-step method to couple transport and reaction (Steefel and Lasaga, 1994; Steefel and MacQuarrie, 1996). A fuller discussion of the advantages and disadvantages of this approach for this kind of problem can be found in Steefel and Lichtner (1998).

## 5. Geometry of reaction fronts in explicit fracture model

Steefel and Lichtner (1998) gave an expression for equal contours of the concentration in an explicit fracture model based on the analytical solution for transport and reaction in a single fracture and adjacent rock matrix. The analytical solution is based on linear kinetics, stationary state conditions, and pure advective transport in the fracture along with pure diffusion in the rock matrix. From the analytical solution (Steefel and Lichtner, 1998), it is apparent that equal contours of the concentration are represented by

$$\frac{x}{\lambda_m} + \frac{z}{\lambda_f} = \text{constant} \quad (14)$$

where  $\lambda_m$  and  $\lambda_f$  are the equilibration length scales in the rock matrix and fracture, respectively. Since the reaction is assumed to be linear, Eq. (14) also corresponds to constant contours of the reaction rate. For a quasi-stationary state system, the lines of constant concentration and reaction rate also mark the position of mineral fronts. This form of the analytical solution for the rock matrix, therefore, can be used to obtain an expression for the geometry of the mineral fronts

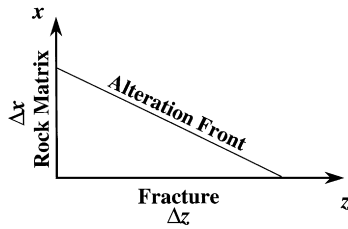


Fig. 2. Schematic representation of rock matrix reaction front geometries in discrete fracture–matrix systems. The reaction front is furthest from the fracture at the inlet where the reactivity of the infiltrating fluid is the highest. Gradual reduction of the reactive capacity of the fluid in the fracture as it migrates downstream causes reaction fronts to converge eventually on the fracture. The slope of reaction front ( $\Delta x/\Delta z$ ) under surface reaction-controlled conditions is approximately equal to the parameter  $\phi D'/\delta v$  where the distances  $\Delta x$  and  $\Delta z$  give the width and length of the alteration envelope respectively (see text and Steefel and Lichtner (1998) for further discussion). Note figure is not drawn to scale.

in the explicit fracture model (Fig. 2). The slope of the quasi-stationary state mineral fronts is then equal to the ratio of the matrix and fracture equilibration lengths

$$\frac{dx}{dz} = -\frac{\lambda_m}{\lambda_f} = -\left(\frac{k_f \lambda_m}{v} + \frac{\phi D'}{v\delta}\right) \quad (15)$$

where  $k_f$  is the rate constant in the fracture. Or we can rewrite this expression in terms of the fracture equilibration length scale in the absence of matrix diffusion to yield

$$\frac{dx}{dz} = -\left(\frac{\lambda_m}{\lambda_f^0} + \frac{\phi D'}{v\delta}\right) \quad (16)$$

Note that the second term in brackets is independent of the kinetic rate constants and depends only on the fracture aperture, matrix porosity and diffusion coefficient, and the fracture fluid velocity. Under surface reaction-controlled conditions, then, the second term dominates, since in general one expects the equilibration length scale in the fracture to be larger than in the rock matrix, yielding

$$\frac{dx}{dz} \approx -\frac{\phi D'}{v\delta} \quad (17)$$

This expression will be used to estimate fracture apertures based on the widths of mineral alteration fronts along fractures at Maqarin, Jordan.

## 6. Hyperalkaline groundwater at maqarin, jordan

At Maqarin, Jordan, hyperalkaline groundwater results from interaction with natural occurrences of portlandite [ $\text{Ca}(\text{OH})_2$ ], the result of in situ combustion of bituminous marls (Alexander et al., 1998; Smellie, 1998). Because of the interest in the long-term effects of groundwater interaction with cement in nuclear waste repositories, the Maqarin area has been intensively studied as a natural analogue site for low-level and intermediate-level waste repositories. Maqarin is located in northern Jordan, close to the Syrian border (Fig. 3) within a stratigraphic sequence consisting of Cretaceous–Tertiary carbonate rocks overlain by Quaternary basalts and soils. The units of principal interest, because they host the portlandite occurrences, are the Cretaceous Muwaqqar formation or bituminous marl formation, and the overlying Lower Tertiary Rijam and Wadi Shallala formations, jointly referred to as the chalky limestone formation. The thickness of the bituminous marl formation is about 220 m in the study area, while the chalky limestone formation ranges from 300–390 m thick. Combustion of bituminous marls within the sequence followed by rehydration and recarbonation reactions locally produced mineralogy analogous to that found in portland cements. This is referred to as the ‘metamorphic zone’, and is restricted to the top of the bituminous marl and the bottom of the chalky limestone formation (Khoury et al., 1998). Groundwater circulating through the metamorphic zone attains chemical compositions very close to those found in cement porewaters, i.e. waters with a very high pH (12.1–13.5) and high  $\text{Ca}^{+2}$  contents (Smellie, 1998). In addition, much of the groundwater flow is through fractures, so the site represents an excellent analogue of the kind of hydrologic and hydrogeochemical conditions expected in the near-field region of a nuclear waste repository.

### 6.1. Hydrologic and hydrogeochemical setting

Regional groundwater flow in the Maqarin area is generally westwards towards the Jordan River valley and north-west towards the Yarmouk River valley (Khoury et al., 1998). Several spring complexes occur in the area, including an Eastern Springs area and a Western Springs area (Fig. 3). On a more local

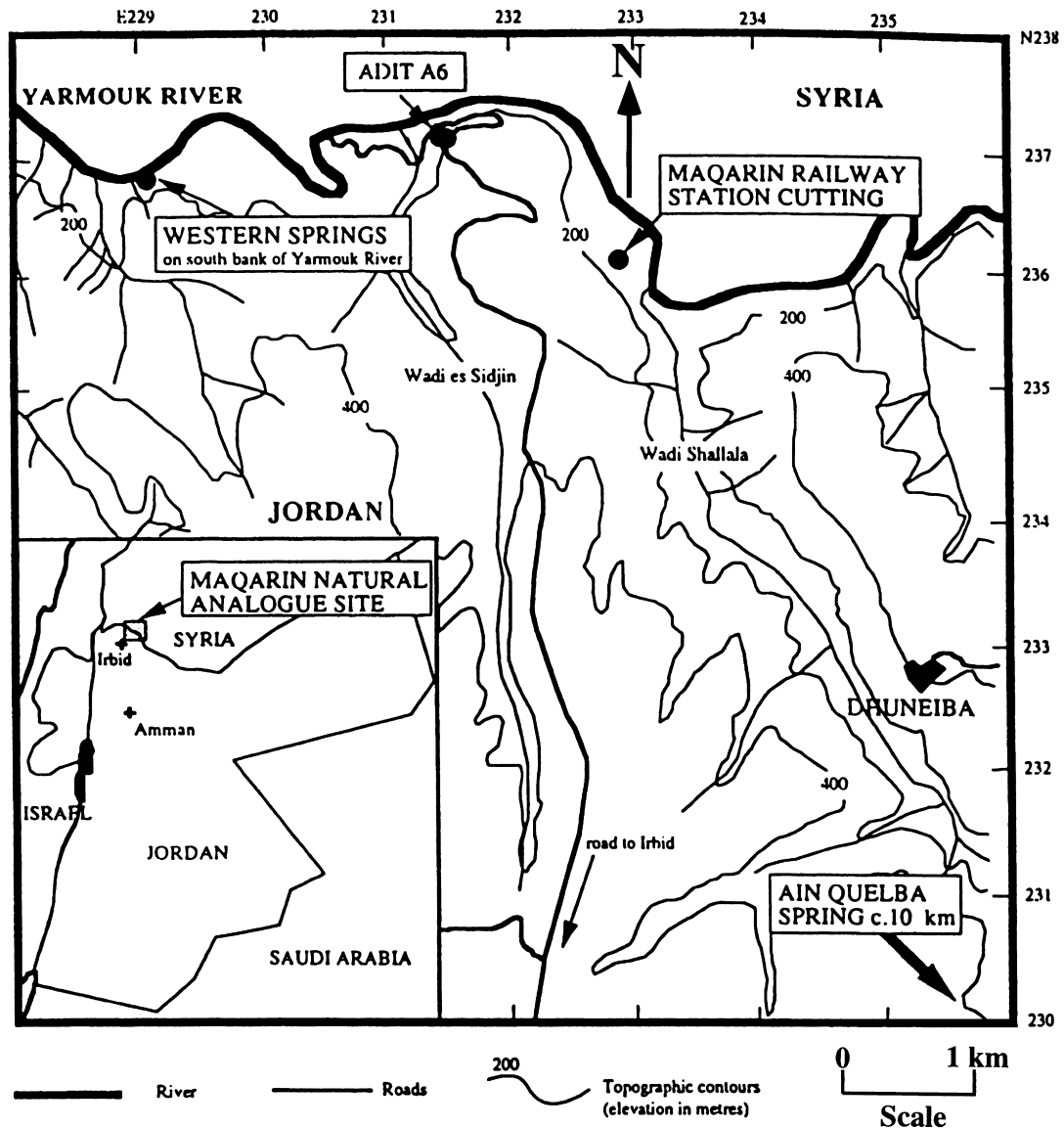


Fig. 3. Location of the Maqarin natural analogue field site. The A-6 adit exposes altered rock and hyperalkaline seeps in the Eastern Springs area and is the focus of this study. After Smellie (1998).

scale, three main groundwater bodies have been identified in the Eastern Springs area, all of which flow northwards towards the Yarmouk River valley (Smellie, 1998): (1) groundwater in a deep confined aquifer in the Amman formation underlying the bituminous marl; (2) groundwater derived from infiltration of meteoric water through the chalky limestone

unit which penetrates down into the metamorphosed bituminous marl, then migrating along the contact between metamorphosed, cement-bearing marls and unmetamorphosed marls; and (3) groundwater infiltrating the chalky limestone directly above the A-6 adit, the site of most of the mineralogic and hydro-geochemical investigations of the Eastern Springs

area. The second type of groundwater gives rise to most of the hyperalkaline spring water observed at the Eastern Springs area. Hyperalkaline groundwater is also observed at the Western Springs area, although part of the flowpath at this locality lies within Quaternary colluvium.

Hyperalkaline groundwater at the Eastern Springs area infiltrates the bituminous marl primarily along fractures, the formation otherwise acting as an aquitard. Khoury et al. (1998) report that hydraulic conductivities based on pumping tests in unfractured portions of the bituminous marl are less than  $10^{-8} \text{ m s}^{-1}$ , while conductivities in fractured marl range as high as  $10^{-7} \text{ m s}^{-1}$ .

Groundwaters within the unmetamorphosed parts of the bituminous marl (Muwaqqar) and chalky limestone (Rijam and Wadi Shallala) formations show near-neutral pH values and range from relatively dilute Ca-Mg-(Na)-HCO<sub>3</sub>-(Cl)-type groundwaters to more strongly mineralized Na-Ca-SO<sub>4</sub>-Cl-type groundwaters (Waber et al., 1998). Isotopic and hydrogeochemical studies of groundwater that has circulated through the metamorphosed (cement-bearing) portion of the Muwaqqar formation suggest that the groundwater is dominantly meteoric and of local origin, initially relatively dilute and with near-neutral pH values (Waber et al., 1998).

There is evidence that the Ca(OH)<sub>2</sub>-rich hyperalkaline springs have been active for some time, since extensive alteration products are observed in fractures and rock matrix bordering fractures. Alteration in the Eastern Springs area is particularly well exposed in the A-6 adit (or tunnel) and has been examined in detail at two points, the M1 and M2 sampling sites (Fig. 4). The host rock at these sampling sites is described by Milodowski et al. (1998) as a clay biomicrite. The mineralogy will be described in greater detail later since this information will be used in constraining the modeling, but we summarize the alteration effects here. Wallrock bordering the fractures is generally leached of calcite, kaolinite, and silica, with porosity immediately adjacent to the fracture increased. Primary silicate and carbonate phases are replaced by fine-grained ettringite [Ca<sub>6</sub>Al<sub>2</sub>(SO<sub>4</sub>)<sub>3</sub>(OH)<sub>12</sub>·26H<sub>2</sub>O] and CSH (hydrated calcium-silicate) phases. Fracture mineralization at the M1 and M2 sites is dominated by an infilling of ettringite with lesser amounts of CSH-phases which

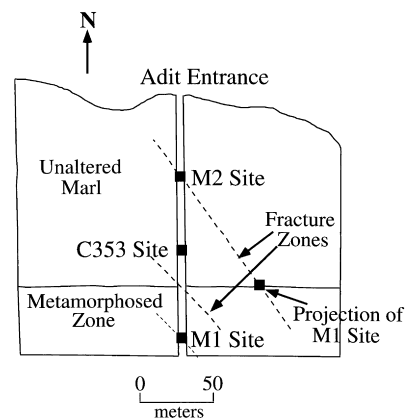


Fig. 4. Map of the A-6 adit in the Eastern Springs area, Maqarin. Note location of the M1 and M2 sampling sites discussed in the text. Also shown is the projection of the M1 site onto the fracture set which crosses the adit at the M2 site. The slope of the local phreatic surface indicates flow is from south-east toward the north-west, approximately parallel to the fracture orientations shown. Modified after Milodowski et al. (1998).

generally postdate the ettringite. Many fractures are filled completely with secondary hyperalkaline reaction products, while other fractures are apparently newly formed, showing little alteration.

#### 6.2. M1 and M2 sampling sites in the A-6 adit, Eastern Springs area

The focus of this study is on a set of fractures exposed in the A-6 adit within the Eastern Springs area at Maqarin (Fig. 4). Extensive hydrogeochemical, isotopic, and mineralogical sampling has been carried out along the fractures at the M1 and M2 sites within the A-6 adit (Alexander et al., 1998; Smellie, 1998). High pH examples include waters from the M1, M2 and M3 sites (Table 1; Waber et al., 1998). Both the M1 and M2 sites are located in the A-6 adit (Fig. 4), while the M3 site is located in the railway cut to the east of the adit (Fig. 3). In each case, pH has been computed on the basis of a titration of hydroxyl ion, considered more reliable than field pH determinations which tend to be consistently higher (Waber, pers. comm., 1998). The groundwaters also show significant concentrations of SO<sub>4</sub><sup>-2</sup> which are attributed to oxidation of pyrite, although gypsum is also present at deeper stratigraphic levels. The highest pH values occur at the M3 site where the groundwater

Table 1  
Compositions of hyperalkaline groundwater from the Eastern Springs area, Maqarin

	M1 Site (molality)	M2 Site (molality)	M3 Site (molality)
OH <sup>-</sup>	$2.48 \times 10^{-2}$	$1.52 \times 10^{-2}$	$3.09 \times 10^{-2}$
Total Al <sup>3+</sup>	$5.19 \times 10^{-6}$	$6.68 \times 10^{-6}$	$5.56 \times 10^{-6}$
Total K <sup>+</sup>	$2.53 \times 10^{-3}$	$3.74 \times 10^{-4}$	$5.07 \times 10^{-4}$
Total Na <sup>+</sup>	$2.05 \times 10^{-3}$	$2.23 \times 10^{-3}$	$2.03 \times 10^{-3}$
Total Ca <sup>2+</sup>	$1.68 \times 10^{-2}$	$1.07 \times 10^{-2}$	$2.01 \times 10^{-2}$
Total Mg <sup>2+</sup>	$4.12 \times 10^{-7}$	$4.12 \times 10^{-7}$	$4.12 \times 10^{-7}$
Total SiO <sub>2</sub> (aq)	$2.56 \times 10^{-7}$	$5.25 \times 10^{-6}$	$1.15 \times 10^{-6}$
Total CO <sub>2</sub>	$6.17 \times 10^{-4}$	$3.67 \times 10^{-4}$	$4.84 \times 10^{-4}$
Total SO <sub>4</sub> <sup>2-</sup>	$3.18 \times 10^{-3}$	$2.84 \times 10^{-3}$	$3.01 \times 10^{-3}$
Total Cl <sup>-</sup>	$1.48 \times 10^{-3}$	$1.92 \times 10^{-3}$	$2.04 \times 10^{-3}$
T (°C)	24.8	20.7	23.2
pH (titr.)	12.30	12.09	12.39
pH (field)	12.67	12.47	12.76

Data kindly provided by N. Waber, Universität Bern, Switzerland.

is at or very close to equilibrium with portlandite. In addition, silica concentrations are very low (well below quartz solubility), strongly suggesting solubility control by a CSH phase. Using the geochemical code PHREEQC (Parkhurst, 1995), Waber et al. (1998) have shown that the M3 geochemistry can be obtained by reacting the local near-neutral Na-HCO<sub>3</sub> groundwater to equilibrium with portlandite, and by reacting lesser amounts of pyrite to yield the elevated SO<sub>4</sub><sup>2-</sup> concentrations. Minor adjustment of Na and K

concentrations are also needed. Similar results were obtained with reaction path calculations using the GIMRT package (Steefel and Yabusaki, 1996), which is also used below to carry out the full 2D reactive transport simulations. The M1 and M2 groundwater analyses show somewhat lower pH values compared to the M3 site (rail cut, see Fig. 3). Although this may be the result of local near-neutral groundwaters simply undergoing less reaction with portlandite and pyrite than at the M3 site, as implied by the reaction path calculations carried out by Waber et al. (1998), we argue below that a more plausible explanation is that the lower pH values at these sampling sites are the result of interaction between the hyperalkaline groundwaters and the fractured clay biomicrite (or marl) downstream of the portlandite occurrences.

A contour map of the phreatic surface in the vicinity of the A-6 adit is shown in Fig. 5. The presence of two local groundwater highs suggest two recharge points, one of which occurs directly above the A-6 adit. Note the location of the A-6 adit within which the M1 and M2 sampling sites occur. Khoury et al. (1998) report that rainfall in the area is about 458 mm year<sup>-1</sup>, most of which apparently makes its way to the water table. The hydraulic head gradient along the trace of the fracture systems exposed in the A-6 adit (here simply the elevation of the water table since the aquifer is unconfined) is about 0.1. Assuming a steady-state groundwater flow system with a

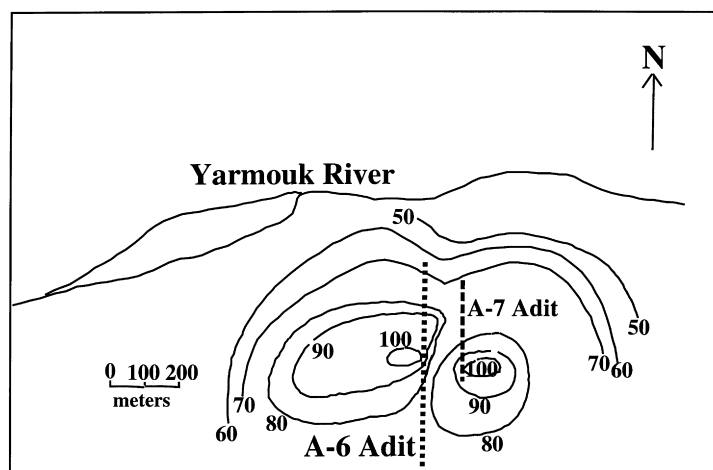


Fig. 5. Contour of the phreatic surface in meters in the vicinity of the A-6 adit, Eastern Springs area at Maqarin, Jordan. Modified after Khoury et al. (1998).

Darcian velocity of  $0.458 \text{ m year}^{-1}$  and a hydraulic head gradient of about 0.1, one calculates a hydraulic conductivity of approximately  $4.5 \text{ m year}^{-1}$  ( $10^{-6.8} \text{ m s}^{-1}$ ). While it is unlikely that all of the rainfall actually becomes recharge, the calculated hydraulic conductivity is close to the range reported by Khoury et al. (1998) based on pumping tests ( $10^{-7}$ – $10^{-9} \text{ m s}^{-1}$ ). The bulk hydraulic conductivity value is only used in determining the number of fractures per meter necessary to transmit the bulk groundwater flow. Actual velocities in the fracture are calculated using the hydraulic head gradient and Eq. (17). It should also be noted that the slope of the water table indicates groundwater flow should be to the northwest, in agreement with the regional pattern of groundwater flow towards the Yarmouk River. According to the hydrologic data, then, the M2 site lies downgradient from the M1 site.

The M1 and M2 sites have been the most intensively studied localities from a mineralogic point of view. According to Alexander et al. (1998), the M1 site represents ‘the most intense fracture mineralization and wallrock alteration observed at Maqarin’. Most of the alteration of the rock matrix at the M1 site occurs within 0.5–4 mm of the fracture. Fine-grained matrix calcite, kaolinite, silica, traces of illite, albite, and organic matter are dissolved. The original mineralogy tends to be completely replaced

by fine-grained secondary phases. Porosity is significantly enhanced within about 1 mm of the fracture. A narrow zone of fine-grained calcite is precipitated at the interface between altered and unaltered marl at the M1 site and at several other nearby sampling localities (Milodowski et al., 1998).

The fracture mineralization at the M1 site is highly complex, reflecting several episodes of fracture filling and reopening (Milodowski et al., 1998). The earliest formed mineralization is aragonite, which is followed by precipitation of a thaumasite–ettringite solid solution and gypsum. Fracture reactivation is followed by various CSH phases, including tobermorite and jennite. Zeolites, which are locally found as the latest stage of mineralization, are not found at the M1 site. Further work on other sample localities within about 20 m of the M1 site (the C353 site, see Fig. 4) indicate a similar paragenesis, with ettringite dominating volumetrically (Fig. 6). The clay biomicrite (marl) alongside the fracture is intensely altered and partly converted to ettringite and thaumasite (Milodowski et al., 1998).

Mineralization both in the fracture and in adjacent wallrock at the M2 site (and nearby localities) is similar in style to the M1 site, differing primarily in the intensity of the alteration. Intense alteration of the rock matrix extends to about 1 mm from the fracture wall, in contrast to nearly 4 mm at the M1 site. Like

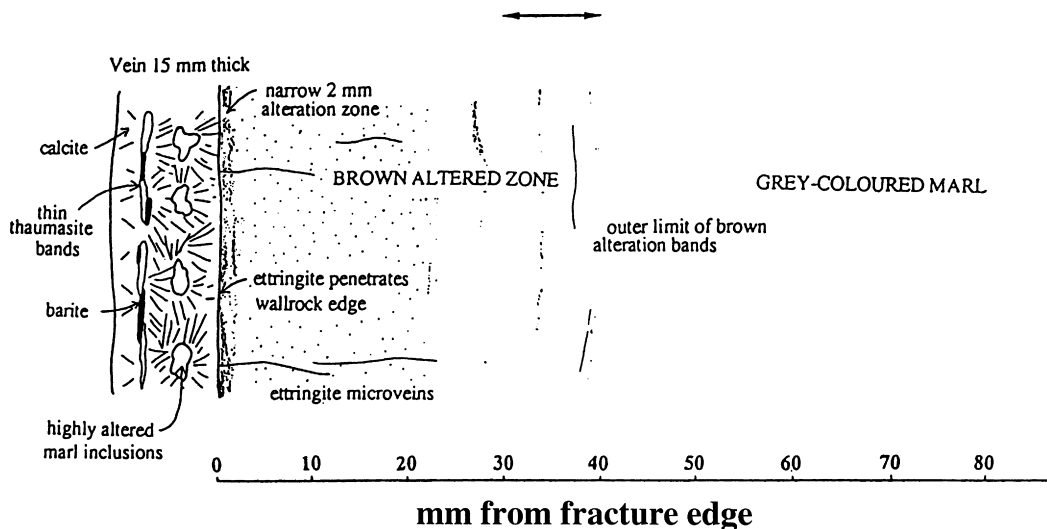


Fig. 6. Rock matrix or wallrock alteration at the C353 site, collected about 20 m from the M1 sampling site (after Milodowski et al., 1998).

the M1 site, however, wallrock replacement is mostly by ettringite which also makes up the bulk of the fracture filling along with lesser CSH phases.

In detail, the fracturing and alteration at all of the localities is extremely complex, with clear evidence for repeated sealing and reopening of fractures. This is also borne out by the observation that some fractures in close proximity to each other may show different fracture infilling. Fracture apertures are highly variable at any one place as well, with active fractures locally showing apertures up to 5 mm. Both sealed and open fractures are observed at the M1 and M2 sites. Locally, the fractures occur as abundant, closely spaced fine anastomosing networks, and at the M1 site, the zone of discharge is actually an array of microfractures covering an area of 0.1–0.2 m<sup>2</sup> (Khoury et al., 1998). As is evident from Fig. 4, the M1 and M2 sites do not lie along the same fracture set, although the argument can be made that fluid moving down the two distinct fracture sets may experience similar histories.

## 7. Modeling the A-6 adit fracture systems

As discussed earlier, fracture sets exposed in the A-6 adit (Eastern Springs area) at Maqarin are oriented approximately N40W, sub-perpendicular to the local hydraulic head contours. The slope of the water table towards the north-west indicates the fracture flow should be from the M1 site towards the M2 site. Calculating a bulk Darcy velocity through the fractured clay biomicrite based on the assumption of steady-state water table elevations indicates a bulk hydraulic conductivity maximum of about 4.5 m year<sup>-1</sup>. Since runoff and evapotranspiration may be 60% of the rainfall, actual hydraulic conductivities could be correspondingly lower. If we assume that the cubic law holds and that the fracture permeability depends on the cube of the fracture aperture and that flow is down a set of parallel fractures whose mean aperture is known, we can calculate velocities in the fracture. The transmissivity of the fractures should depend on the harmonic mean of the fracture aperture (weighting the results towards the minimum aperture over the length of the fracture system). The ideal way to proceed would be to carry out one or more tracer tests to determine fracture velocities directly. To our

knowledge, however, this information is not available and therefore we rely on the change in the thickness of the alteration envelope bordering fractures at the M1 site (about 4 mm) to the width of about 1 mm observed at the M2 site 100 meters downgradient as a way of constraining the fracture aperture and velocity. Even though the two sampling sites do not lie along the same fracture set, we argue that groundwater flowing down the fractures may experience similar histories. To carry out the analysis, therefore, we project the M1 sampling site onto the fracture which crosses the adit at the M2 site (Fig. 4). We make use of the expression for the geometry of wallrock alteration zones derived in Steefel and Lichtner (1998) and given previously (Eq. (17)). Chambers et al. (1998) give the effective diffusion coefficient ( $D' = \tau D_w$ ) at Maqarin as  $3 \times 10^{-11} \text{ m}^2 \text{ s}^{-1}$  and the average porosity of the clay biomicrite or marl as 30%. Assuming surface reaction-control, the geometry of the wallrock alteration zones (see Fig. 2) implies the following relation

$$\frac{\Delta z}{\Delta x} = 100/0.003 = \frac{v\delta}{\phi D'} \quad (18)$$

where  $\Delta z$  is the distance along the fracture between the projection of the M1 site (Fig. 4) and the M2 site and  $\Delta x$  is the change in the width of the rock matrix alteration envelope between these two sites. Using the values for the porosity and the effective diffusion coefficient given above gives a value of  $v\delta$  of  $3 \times 10^{-7} \text{ m}^2 \text{ s}^{-1}$ . Combining this information with the expression for the mean flow velocity in the fracture given in Eq. (7), we obtain the following expression

$$\delta v = \phi D' \frac{\Delta z}{\Delta x} = \frac{\delta^3 \rho g}{3\mu} \left| \frac{\partial h}{\partial z} \right| \quad (19)$$

or solving for the fracture aperture half-width,

$$\delta = \left[ \frac{3\mu\phi D' \Delta z}{\rho g \Delta x} \left| \frac{\partial h}{\partial z} \right|^{-1} \right]^{1/3} \quad (20)$$

Using the approximate hydraulic head gradient of 0.1 obtained from Fig. 5, this yields a fracture aperture half-width of 0.097 mm and a fracture velocity of 267 m day<sup>-1</sup>. If the fracture permeability consists of a set of equally spaced fractures with this aperture, a bulk hydraulic conductivity of 4.5 m year<sup>-1</sup> (corresponding to a bulk permeability of  $1.4 \times 10^{-14} \text{ m}^2$ )

requires fractures spaced about 44 m apart (see Eq. (3)). This is close to the distance between the M2 fracture set and the nearest fracture set to the southwest (Fig. 4).

This calculation, which is based on the assumption that the cubic law applies, gives fracture velocities that appear high. There is considerable field evidence questioning the validity of the cubic law (Raven et al., 1988). Raven et al. (1988), for example, show that tracer tests carried out at the Chalk River Nuclear Laboratories yield velocities in the fractures which are 4–10 times slower than those calculated based on pump tests assuming the cubic law applies. One could argue, therefore, that velocities in the fractures exposed in the A-6 adit may be as low as 26 m day<sup>-1</sup>, although one or more tracer tests would be required to verify this. In order for the expression for alteration front geometry to apply, this would require an effective aperture 10 times larger. Clearly, the cubic law could not be applied in this case, since it would predict either extremely high bulk hydraulic conductivities or very widely spaced fractures, neither of which are observed in the Eastern Springs area. One might rationalize the use of a lower fracture velocity and larger aperture by pointing out that the aperture as it appears in the cubic law should be a harmonic mean aperture, weighted towards the smaller values which control the overall flow rate through the fracture. In contrast, the aperture which appears in the equation for alteration front geometry (Eq. (17)) determines the volume of fluid whose concentration must be adjusted by diffusion through the fracture wall. This might be better approximated by an arithmetic mean. As pointed out by Raven et al. (1988), zones of relatively immobile water in wider portions of a non-smooth fracture store solute mass and must be considered in the overall solute mass balance, even though they don't contribute significantly to the fluid flux through the fracture. This effect, however, is not explicitly considered in the present model.

The change in the thickness of the rock matrix alteration zone as a function of distance along the fracture is only one of the parameters that can be used to constrain the fracture velocity and aperture. We can also check whether the numerical simulations can match the solution chemistry (especially the pH) of the springs exposed in the adit. The

consistency (or lack thereof) between the pH of the active springs and the rock matrix alteration thicknesses gives us an additional control on the validity of the model.

### 7.1. Thermodynamic and kinetic data base

Geochemical reactions included in the simulations of Maqarin are given in Table 2 and Table 3. Most of the equilibrium constants are taken from the EQ3/EQ6 database (V8.R5 release). A number of the equilibrium constants for reactions involving high pH phases, including the minerals ettringite, tobermorite, Si-hydrogarnet, tricarboaluminate, and hydrocalcite, are taken from a database compilation (F. Glasser, pers. comm.). One-dimensional reaction–diffusion calculations were carried out at an early stage with a larger list of possible solid phases.

Table 2

Reactions and equilibrium constants for aqueous species used in the calculations.

Reaction	Log $K_{eq}$
$\text{OH}^- + \text{H}^+ \rightleftharpoons \text{H}_2\text{O}$	14.00
$\text{HCO}_3^- \rightleftharpoons \text{CO}_3^{2-} + \text{H}^+$	- 10.33
$\text{CO}_2(\text{aq}) + \text{H}_2\text{O} \rightleftharpoons \text{CO}_3^{2-} + 2\text{H}^+$	- 16.67
$\text{NaHCO}_3(\text{aq}) \rightleftharpoons \text{CO}_3^{2-} + \text{H}^+ + \text{Na}^+$	- 10.48
$\text{NaCO}_3^- \rightleftharpoons \text{CO}_3^{2-} + \text{Na}^+$	- 0.51
$\text{Al}(\text{OH})^{+2} + \text{H}^+ \rightleftharpoons \text{Al}^{+3} + \text{H}_2\text{O}$	4.96
$\text{Al}(\text{OH})_2^+ + 2\text{H}^+ \rightleftharpoons \text{Al}^{+3} + 2\text{H}_2\text{O}$	10.60
$\text{Al}(\text{OH})_3(\text{aq}) + 3\text{H}^+ \rightleftharpoons \text{Al}^{+3} + 3\text{H}_2\text{O}$	16.16
$\text{Al}(\text{OH})_4^- + 4\text{H}^+ \rightleftharpoons \text{Al}^{+3} + 4\text{H}_2\text{O}$	22.88
$\text{H}_2\text{SiO}_4^{2-} + 2\text{H}^+ \rightleftharpoons \text{SiO}_2(\text{aq}) + 2\text{H}_2\text{O}$	22.96
$\text{H}_3\text{SiO}_4^- + \text{H}^+ \rightleftharpoons \text{SiO}_2(\text{aq}) + 2\text{H}_2\text{O}$	9.95
$\text{NaOH}(\text{aq}) + \text{H}^+ \rightleftharpoons \text{Na}^+ + \text{H}_2\text{O}$	14.80
$\text{NaSO}_4^- \rightleftharpoons \text{Na}^+ + \text{SO}_4^{2-}$	- 0.82
$\text{MgCO}_3(\text{aq}) \rightleftharpoons \text{CO}_3^{2-} + \text{Mg}^{+2}$	- 2.98
$\text{MgHCO}_3^+ \rightleftharpoons \text{CO}_3^{2-} + \text{Mg}^{+2} + \text{H}^+$	- 11.37
$\text{MgOH}^+ + \text{H}^+ \rightleftharpoons \text{Mg}^{+2} + \text{H}_2\text{O}$	11.79
$\text{MgCl}^+ \rightleftharpoons \text{Mg}^{+2} + \text{Cl}^-$	0.13
$\text{MgH}_2\text{SiO}_4(\text{aq}) + 2\text{H}^+ \rightleftharpoons \text{Mg}^{+2} + \text{SiO}_2(\text{aq}) + 2\text{H}_2\text{O}$	17.48
$\text{MgH}_3\text{SiO}_4^+ + \text{H}^+ \rightleftharpoons \text{Mg}^{+2} + \text{SiO}_2(\text{aq}) + 2\text{H}_2\text{O}$	8.54
$\text{MgSO}_4(\text{aq}) \rightleftharpoons \text{SO}_4^{2-} + \text{Mg}^{+2}$	- 2.41
$\text{CaH}_2\text{SiO}_4(\text{aq}) + 2\text{H}^+ \rightleftharpoons \text{Ca}^{+2} + \text{SiO}_2(\text{aq}) + 2\text{H}_2\text{O}$	18.56
$\text{CaH}_3\text{SiO}_4^+ + \text{H}^+ \rightleftharpoons \text{Ca}^{+2} + \text{SiO}_2(\text{aq}) + 2\text{H}_2\text{O}$	8.79
$\text{Ca}(\text{H}_3\text{SiO}_4)_2(\text{aq}) + 2\text{H}^+ \rightleftharpoons \text{Ca}^{+2} + 2\text{SiO}_2(\text{aq}) + 4\text{H}_2\text{O}$	15.05
$\text{CaHCO}_3^+ \rightleftharpoons \text{CO}_3^{2-} + \text{Ca}^{+2} + \text{H}^+$	- 11.38
$\text{CaOH}^+ + \text{H}^+ \rightleftharpoons \text{Ca}^{+2} + \text{H}_2\text{O}$	12.85
$\text{CaSO}_4(\text{aq}) \rightleftharpoons \text{Ca}^{+2} + \text{SO}_4^{2-}$	- 2.11
$\text{KOH}(\text{aq}) + \text{H}^+ \rightleftharpoons \text{K}^+ + \text{H}_2\text{O}$	14.46
$\text{KSO}_4^- \rightleftharpoons \text{K}^+ + \text{SO}_4^{2-}$	- 0.88

Table 3

Reactions and equilibrium constants for minerals used in the calculations.

Mineral	Reaction	Log $K_{eq}$
Calcite	$\text{CaCO}_3 \rightleftharpoons \text{Ca}^{+2} + \text{CO}_3^{-2}$	– 8.48
Muscovite	$\text{KAl}_3\text{Si}_3\text{O}_{10}(\text{OH})_2 + 10\text{H}^+ \rightleftharpoons \text{K}^+ + 3\text{SiO}_2(\text{aq}) + 3\text{Al}^{+3} + 6\text{H}_2\text{O}$	13.59
Kaolinite	$\text{Al}_2\text{Si}_2\text{O}_5(\text{OH})_4 + 6\text{H}^+ \rightleftharpoons 2\text{SiO}_2(\text{aq}) + 2\text{Al}^{+3} + 5\text{H}_2\text{O}$	6.81
Chalcedony	$\text{SiO}_2 \rightleftharpoons \text{SiO}_2(\text{aq})$	– 3.73
Sepiolite	$\text{Mg}_4\text{Si}_6\text{O}_{15}(\text{OH})_2 \cdot 6\text{H}_2\text{O} + 8\text{H}^+ \rightleftharpoons 6\text{SiO}_2(\text{aq}) + 4\text{Mg}^{+2} + 11\text{H}_2\text{O}$	30.44
Brucite	$\text{Mg}(\text{OH})_2 + 2\text{H}^+ \rightleftharpoons \text{Mg}^{+2} + 2\text{H}_2\text{O}$	16.30
Ettringite	$\text{Ca}_6\text{Al}_2(\text{SO}_4)_3(\text{OH})_{12} \cdot 26\text{H}_2\text{O} + 12\text{H}^+ \rightleftharpoons 2\text{Al}^{+3} + 6\text{Ca}^{+2} + 3\text{SO}_4^{-2} + 38\text{H}_2\text{O}$	57.81
Tobermorite	$\text{Ca}_5\text{Si}_6\text{O}_{12}(\text{OH})_{10} + 10\text{H}^+ \rightleftharpoons 6\text{SiO}_2(\text{aq}) + 5\text{Ca}^{+2} + 10\text{H}_2\text{O}$	64.35
Portlandite	$\text{Ca}(\text{OH})_2 + 2\text{H}^+ \rightleftharpoons \text{Ca}^{+2} + 2\text{H}_2\text{O}$	22.56
Gypsum	$\text{CaSO}_4 \cdot 2\text{H}_2\text{O} \rightleftharpoons \text{Ca}^{+2} + \text{SO}_4^{-2} + 2\text{H}_2\text{O}$	– 4.48
Si-hydrogarnet	$\text{Ca}_3\text{Al}_2\text{SiO}_4(\text{OH})_8 + 12\text{H}^+ \rightleftharpoons 2\text{Al}^{+3} + \text{SiO}_2(\text{aq}) + 3\text{Ca}^{+2} + 10\text{H}_2\text{O}$	69.37
Tricarboaluminate	$\text{Ca}_6\text{Al}_2(\text{CO}_3)(\text{OH})_{12} \cdot 24\text{H}_2\text{O} + 12\text{H}^+ \rightleftharpoons 2\text{Al}^{+3} + 3\text{CO}_3^{-2} + 6\text{Ca}^{+2} + 36\text{H}_2\text{O}$	51.60
Hydrotalcite	$\text{Mg}_4\text{Al}_2\text{O}_4(\text{OH})_6 + 14\text{H}^+ \rightleftharpoons 2\text{Al}^{+3} + 4\text{Mg}^{+2} + 10\text{H}_2\text{O}$	75.44
Friedel-salt	$\text{Ca}_4\text{Al}_2\text{Cl}_2(\text{OH})_{12} + 12\text{H}^+ \rightleftharpoons 2\text{Al}^{+3} + 4\text{Ca}^{+2} + 2\text{Cl}^-$	70.13
Hillebrandite	$\text{Ca}_2\text{SiO}_3(\text{OH})_2 \cdot 0.17\text{H}_2\text{O} + 4\text{H}^+ \rightleftharpoons \text{SiO}_2(\text{aq}) + 2\text{Ca}^{+2} + 3.17\text{H}_2\text{O}$	35.30
Foshagite	$\text{Ca}_4\text{Si}_3\text{O}_9(\text{OH})_2 \cdot 0.5\text{H}_2\text{O} + 8\text{H}^+ \rightleftharpoons 3\text{SiO}_2(\text{aq}) + 4\text{Ca}^{+2} + 5.5\text{H}_2\text{O}$	63.00

The present list includes those secondary minerals which formed somewhere within the domain at some time in the simulations. Many of the equilibrium constants for the high pH secondary phases are associated with significant uncertainty. For example, Reardon (1992) reports the log of the equilibrium constant for the ettringite dissolution reaction as 57.81 while F. Glasser (pers. comm.) reports a value of 55.22.

The values of the equilibrium constants for hillebrandite and portlandite were changed from previously reported values on the basis of the Maqarin water chemistry. The extremely low silica concentrations at both the M1 and M3 sites (well below quartz solubility, see Table 1) strongly suggest that they are controlled by a CSH-phase. However, none of the reported equilibrium constants for CSH-phases were low enough to give the observed silica concentration. The closest was hillebrandite, so the log of the equilibrium constant for hillebrandite was revised to 35.3 (compared with a previously reported low value of 36.3). The equilibrium constant for portlandite was also slightly revised upward to make it in equilibrium with the groundwater reported at the M3 site (from 22.55 to 22.66).

Intrinsic rate constants, including their pH dependence, are given in Table 4 and are mostly taken from the excellent summary of silicate mineral weathering rates edited by White and Brantley (1995).

References to the original source of data are given in the table.

### 7.2. Initial and boundary conditions for A-6 adit simulations

Initial and boundary conditions must also be specified in order to carry out a full multicomponent reactive transport calculation. As a boundary condition, we use a slightly modified version of the M3 site groundwater (Table 5; see Table 1 for original analysis) collected at the railway seepage shown in Fig. 3. This particular groundwater sample comes from a site some distance from the A-6 adit, so its use as a boundary condition in the A-6 adit fractures is hypothetical. As discussed previously and in Waber et al. (1998), this groundwater composition can be obtained by reacting the local near-neutral pH Na-HCO<sub>3</sub> groundwater to equilibrium with portlandite and then by oxidizing sufficient pyrite to raise the SO<sub>4</sub><sup>-2</sup> concentration. The principal modifications we have made to the measured M3 compositions involve species like aluminum and inorganic carbon which are most subject to analytical error. We calculate aluminum by assuming the groundwater is in equilibrium with muscovite while total carbonate is calculated based on equilibrium with calcite. Solution pH is calculated from the acid titration data. Use of the field-determined pH results in significant supersaturation

Table 4  
Reaction rate constants and maximum reactive surface areas used for mineral dissolution and precipitation reactions

Mineral	Log $k_{\text{neut}}$ (mol m <sup>-2</sup> s <sup>-1</sup> )	Log $k_{\text{acid}}$ (mol m <sup>-2</sup> s <sup>-1</sup> )	$n_{\text{acid}}$	Log $k_{\text{basic}}$ (mol m <sup>-2</sup> s <sup>-1</sup> )	$n_{\text{basic}}$	Reference	Surface area (m <sup>2</sup> m <sup>-3</sup> )
Calcite	- 6.19					<sup>a</sup>	6000
Muscovite		- 11.38	0.39	- 11.91	0.22	<sup>b</sup>	$5.7 \times 10^5$
Kaolinite		- 11.58	0.17	- 10.88	0.54	<sup>c</sup>	$5.7 \times 10^6$
Chalcedony	- 13.39			- 10.20	0.3	<sup>d</sup>	$5.3 \times 10^3$
Sepiolite	-11.00					<sup>e</sup>	100
Brucite	-8.00					<sup>e</sup>	100
Ettringite	-8.00					<sup>e</sup>	100
Hillebrandite	-8.00					<sup>e</sup>	100
Si-hydrogarnet	-8.00					<sup>e</sup>	100
Foshagite	-8.00					<sup>e</sup>	100
Tobermorite	-8.00					<sup>e</sup>	100
Portlandite	-8.00					<sup>e</sup>	100
Tricarboaluminate	-8.00					<sup>e</sup>	100
Hydrocalcite	-8.00					<sup>e</sup>	100
Friedel-salt	-8.00					<sup>e</sup>	100
Gypsum	-8.00					<sup>e</sup>	100

$k_{\text{neut}}$  refers to the pH-independent rate constant, while  $k_{\text{acid}}$  and  $k_{\text{basic}}$  refer to the H<sup>+</sup>- and OH<sup>-</sup>-dependent rate constants, respectively.  $n_{\text{acid}}$  and  $n_{\text{basic}}$  refer to the exponential dependence of the reaction rate on H<sup>+</sup> and OH<sup>-</sup> (i.e. the reaction order), respectively.

<sup>a</sup>Chou et al. (1989).

<sup>b</sup>Data from experimental study of Knauss and Wolery (1989) at 70°C, corrected using an activation energy of 22 kJ mol<sup>-1</sup> (Nagy, 1995).

<sup>c</sup>Data from Carroll-Webb and Walther (1988) at 25°C, pH dependence refitted.

<sup>d</sup>Using the rate constant and pH dependence for quartz in Dove (1995).

<sup>e</sup>Rate constant chosen to be faster than dissolution of primary minerals.

Table 5

Solute concentrations and constraints for groundwater which has circulated through the 'metamorphic' (portlandite-bearing) zone at the Eastern Springs, Maqarin

	Concentration (mol l <sup>-1</sup> )	Constraint
OH <sup>-</sup>	$3.09 \times 10^{-2}$	Titration
Total Al <sup>3+</sup>	$9.23 \times 10^{-9}$	Ettringite Equilibrium
Total K <sup>+</sup>	$5.07 \times 10^{-4}$	Chemical analysis
Total Na <sup>+</sup>	$2.03 \times 10^{-3}$	Chemical analysis
Total Ca <sup>2+</sup>	$2.01 \times 10^{-2}$	Chemical analysis
Total Mg <sup>2+</sup>	$2.34 \times 10^{-8}$	Brucite Equilibrium
Total SiO <sub>2</sub> (aq)	$1.15 \times 10^{-6}$	Chemical analysis
Total CO <sub>2</sub>	$1.00 \times 10^{-6}$	Calcite Equilibrium
Total SO <sub>4</sub> <sup>2-</sup>	$3.01 \times 10^{-3}$	Chemical analysis
Total Cl <sup>-</sup>	$2.04 \times 10^{-3}$	Chemical analysis
T (°C)	25	
I (M)	$5.55 \times 10^{-2}$	Computed
pH	12.39	Computed
log PCO <sub>2</sub>	- 13.00	Computed
Alkalinity	$3.39 \times 10^{-2}$	Computed

This composition is a modification of the M3 water reported in Table 1 and is used as a boundary condition in the simulations.

with respect to portlandite, while the pH based on hydroxyl ion titration results in a near-equilibrium solution. As an initial condition, we use one of the near-neutral pH, Na-HCO<sub>3</sub> groundwaters (sampling site M6, not shown) which is similar to the composition used to obtain an approximation of the M3 water after reacting with portlandite and pyrite (Table 6). The results are not particularly sensitive, however, to the details of the near-neutral pH groundwater, since this water tends to be flushed out of the system by the infiltration of the hyperalkaline groundwater.

Mineral volume fractions in the clay biomicrite rock matrix are variable in detail, as shown by the careful study of Milodowski et al. (1998). We use the average values for porosity and mineral abundances given by Chambers et al. (1998) (Table 7).

### 7.3. One-dimensional diffusion–reaction calculations

One-dimensional diffusion–reaction calculations are used to estimate primary mineral reactive surface areas based on alteration zone widths observed in the

Table 6  
Solute concentrations and constraints for the Maqarin pore water used as an initial condition in the calculations

	Concentration (mol l <sup>-1</sup> )	Constraint
Total Al <sup>3+</sup>	1.08 × 10 <sup>-8</sup>	Muscovite equilibrium
Total K <sup>+</sup>	9.20 × 10 <sup>-5</sup>	Chemical analysis
Total Na <sup>+</sup>	2.02 × 10 <sup>-4</sup>	Chemical analysis
Total Ca <sup>2+</sup>	6.88 × 10 <sup>-4</sup>	Calcite equilibrium
Total Mg <sup>2+</sup>	2.23 × 10 <sup>-4</sup>	Chemical analysis
Total SiO <sub>2</sub> (aq)	1.70 × 10 <sup>-4</sup>	Chemical analysis
Total CO <sub>2</sub>	3.56 × 10 <sup>-3</sup>	Chemical analysis
Total SO <sub>4</sub> <sup>2-</sup>	3.00 × 10 <sup>-3</sup>	Chemical analysis
Total Cl <sup>-</sup>	5.90 × 10 <sup>-4</sup>	Chemical analysis
T (°C)	25	
I (M)	2.15 × 10 <sup>-2</sup>	Computed
pH	7.77	Field measurement
logP <sub>CO<sub>2</sub></sub>	-2.41	Computed
Alkalinity	3.46 × 10 <sup>-3</sup>	Computed

The chemistry is slightly modified from an analysis of a water from the M6 sampling site.

field. As is evident from the analytical solution for pure diffusive transport and kinetically-controlled mineral dissolution and precipitation (Lichtner, 1988; Steefel and Lichtner, 1998), the equilibration length scale,  $\lambda_m$ , in the rock matrix depends on the rate of diffusive transport relative to the effective rate constant (including both the intrinsic rate constant and the mineral reactive surface area)

$$\lambda_m = \sqrt{\frac{\phi D'}{k_m}} \quad (21)$$

In the transient stage before the primary minerals in the rock have dissolved completely at any point within the domain, the equilibration length scale determines the width of the alteration zone, with

Table 7

Initial modal composition of Maqarin rock matrix used in this study.

Mineral	Volume (%)
Calcite	49.0
Muscovite	1.4
Non-reactive	12.6
Kaolinite	3.5
Chalcedony	3.5
Porosity	30.0

smaller effective rate constants,  $k_m$ , resulting in correspondingly larger alteration zones.

The intrinsic rate constants (in units of mol m<sup>-2</sup> mineral s<sup>-1</sup>) used in the calculation are given in Table 4. Values for mineral reactive surface areas are also needed. Many studies of geochemical reaction rates in the field have assumed that mineral reactive surface areas are known (as they are in controlled laboratory studies) and have attempted to determine intrinsic rate constants in the field (mole per unit surface area per time) (e.g. Drever and Clow, 1995; White, 1995). However, in natural porous media, the hydrologically accessible reactive surface area appears to be much more poorly known than the intrinsic rate constants themselves. In this study, therefore, we assume that laboratory-determined intrinsic rate constants are known (even though there is clearly a level of uncertainty associated with these) and we use the available information to attempt to constrain mineral reactive surface areas.

In paleo-field systems dominated by fluid flow, it is often difficult to use this approach since the rate of fluid flow tends to be poorly known. The rate of diffusion through porous media, however, may be known with better precision, suggesting that field occurrences of diffusion–reaction systems may provide better natural settings for estimating in situ reaction rates than do paleo-flow and reaction systems. Alternatively, the rate of diffusion can be determined directly in the laboratory assuming the physical properties of the rock have not changed significantly from when the alteration took place. In this study we rely on the effective diffusion coefficient in porous media ( $D'$ ) reported by Chambers et al. (1998) and use one-dimensional reactive transport calculations to estimate the appropriate values for reactive surface area needed to match the observed alteration zone widths in the rock matrix bordering fractures at Maqarin.

As a preliminary estimate for the maximum possible reactive surface area of the primary minerals, we use either typical specific surface areas reported for the minerals of interest (normally determined by BET measurements and reported in units of m<sup>2</sup> g<sup>-1</sup>), or we use a geometric estimate based on grain size. Maximum specific surface areas used are given in Table 4. Simulations are then carried out by varying the reactive surface areas of the primary minerals

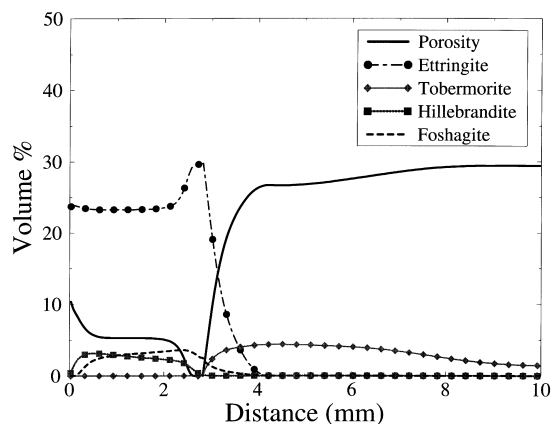


Fig. 7. Secondary mineral volume percentages at 50 years calculated using reactive surface areas 1/5 of the maximum values given in Table 4.

from these maximum values. We expect that these values provide an upper limit for reactive surface area, because not all of the minerals physically present in the rock will be exposed to the pore fluid (i.e. not all of the mineral surface area is hydrologically accessible). Reactive surface areas for secondary minerals are very poorly known (Steefel and Van Cappellen, 1990). If the rate constants for secondary mineral precipitation reactions are chosen sufficiently large that near-equilibrium results (i.e. the dissolution of primary minerals is the rate-limiting step), then the results are not particularly sensitive to the value of the reactive surface area used in the simulation.

The one-dimensional diffusion–reaction calculations are carried out using the boundary condition given in Table 5 as a Dirichlet or fixed concentration condition. A no-flux boundary is assumed at 0.2 m distance from the fracture. Fig. 7 shows secondary mineral volume percentages plotted vs distance in millimeters from the fracture wall for a simulation using primary mineral surface areas one fifth of their maximum values given in Table 4. All of the simulations (regardless of what values for the reactive surface areas are used) predict that ettringite is the major secondary mineral which forms, in agreement with observations of both rock matrix alteration and fracture filling at the Eastern Springs area (Fig. 7). Lesser amounts of foshagite and hillebrandite (both CSH phases) precipitate close to the fracture. Together with ettringite, they cause the porosity in

the rock matrix to go to zero in as little as 10–50 years, depending on the reactive surface areas used in the simulations. Observations from the Eastern Springs area (summarized by Alexander et al., 1998; Milodowski et al., 1998) indicate a complicated history of alteration, including some calcite dissolution and precipitation which is not predicted by the modeling. In simulations of the Swiss low-level site reported in Steefel and Lichtner (1994), calcite and brucite precipitated at the expense of dolomite, forming a narrow cemented zone some distance from the fracture wall. This produces a pattern very similar to what is observed along many of the Maqarin fractures. While mixing of pore water via diffusion will tend to precipitate calcite, the precipitation front will migrate away from the fracture as the relatively small quantity of dissolved carbonate in the pore fluid is locally exhausted. The calcite precipitation mechanism, therefore, requires the dissolution of a carbonate phase to mix with the carbonate-depleted hyperalkaline pore fluid. Dolomite, however, is not reported in most of the exposures examined in the Eastern Springs area (Alexander et al., 1998; Milodowski et al., 1998). It is possible that the dissolving phase is a Mg-rich, more soluble foraminiferal calcite (there is clear textural evidence of dissolution), while the calcite which precipitates in a narrow band millimeters from the fracture may be a lower-Mg calcite in equilibrium with the local groundwater, but no information to suggest that this is the case is available.

As a constraint on the reaction rates, we use the alteration zone widths reported for the M1 sampling site in the A-6 adit at Maqarin. Alexander et al. (1998) reported that intense alteration widths bordering the fracture range from 1 to 4 mm. Fig. 8 shows the porosity of the rock matrix after 50 years for a range of reactive surface areas. By 50 years, the porosity is completely cemented locally, so no further broadening of the alteration envelope occurs. The porosity evolution is primarily the result of precipitation of ettringite with lesser volumes of CSH phases. The simulations indicate that the best fit with the mineralogic data is obtained with reactive surface areas within about one order of magnitude of estimates based on either BET measurements or geometry (i.e. the maximum values). Using reactive surface areas more than one order of magnitude below these values results in widths of strongly altered rock greater than

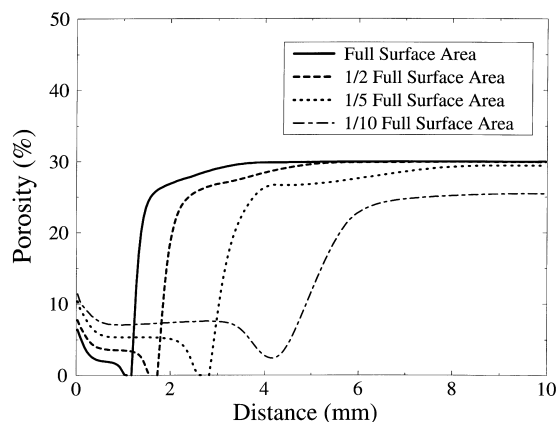


Fig. 8. One-dimensional reaction–diffusion simulations used to estimate values for primary mineral reactive surface areas based on alteration zone width. Intense alteration at the M1 sampling site occurs within about 4 mm of the fracture wall (Alexander et al., 1998), suggesting that reactive surface areas within about 1 order of magnitude of the maximum values given in Table 4 are needed.

1 cm, significantly more than the 4 mm observed at the M1 site.

#### 7.4. Two-dimensional simulations of discrete fractures at Maqarin

Two-dimensional simulations of multicomponent reactive transport are now used to interpret chemical compositions of seepages from fractures in the A-6 adit. The numerical simulations have the advantage of being able to include the time dependence of the entire process, since mineral precipitation and dissolution are expected to modify substantially the physical properties of the fracture–matrix system. Of particular interest is whether the physical parameters used to match the solution composition at the M1 and M2 sampling sites are compatible with the parameters deduced from the change in the width of alteration bordering fractures using Eq. (20). If the simulations are able to match both the alteration zone thicknesses and the chemical composition of the ground water actively circulating through the fracture system, then there is some basis for confidence that the model is capturing at least the first-order behavior of the reactive flow system.

As a first attempt at matching the pH values reported from sampling sites in the A-6 adit (the M1

and M2 sites), we use the hydrologic parameters deduced from the change in alteration zone thickness as a function of distance downstream along the fracture (an aperture of 0.194 mm and a fracture velocity of 267 m day<sup>-1</sup>). Using these values, we obtain too large a drop in pH over the distance between the M1 and M2 sites, indicating that a higher flow velocity and/or larger aperture is needed to match the data. We obtain the best fit to the measured pH at the M1 and M2 sites by using an aperture of 0.22 mm and a velocity in the fracture of 341 m day<sup>-1</sup>. This requires a fracture spacing of about 66 m in order to account for the bulk hydraulic conductivity observed at the site. Again, this is reasonably close to typical distances between major fractures observed in the A-6 adit (Fig. 4). These calculated values of the fracture velocity and aperture are within about 13% of the value based on the change in rock matrix alteration thickness.

Reaction-induced porosity and permeability change in both the fracture and the rock matrix result in some complex time-dependent behavior. The system behavior is highly sensitive to the rate constants used, although the constraint that they reproduce the observed alteration zone thickness limits the range of values that the parameters may take. Reactive surface areas of primary minerals are assumed to be 1/5 of the maximum values given in Table 4. The simulations predict that if the rate constants and reactive surface areas for secondary minerals are the same in the fracture and the matrix, the matrix will seal first. This causes the slope of both the reaction front boundaries and lines of equal concentration to approach 0 (i.e. to become sub-parallel to the fracture) with time [Fig. 9(a)]. One can view this as the result of the numerator of the expression  $\Delta x/\Delta z = \phi D/v\delta$  approaching zero faster than the denominator. This causes a migration of all reaction fronts downstream with time and no sealing of the fracture [Fig. 10(a)]. Insofar as the natural analogue results apply to the performance of cement-bearing nuclear waste repositories, this is a worst case scenario in which radionuclides might eventually migrate through the near-field with essentially no retardation (Steefel and Lichtner, 1994). However, the observation at Maqarin is that the fractures eventually seal themselves, although an initial downstream migration due to rock matrix cementation is not ruled out by the data. In order to have the

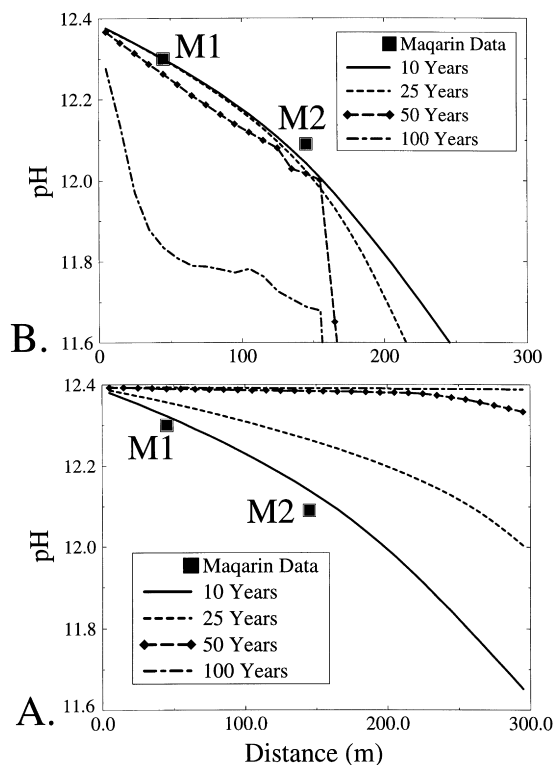


Fig. 9. pH vs distance along the fracture. (a) Case where reactive surface areas for secondary minerals in the rock matrix are equal to those in the fracture. Sealing of rock matrix before the fracture causes downstream propagation of hyperalkaline plume. (b) Case where reactive surface areas for secondary minerals in the rock matrix are 1/10 of the values in the fracture. More rapid precipitation in the fracture causes it to seal before the rock matrix, resulting in an upstream collapse of the hyperalkaline plume.

fractures seal, either a porosity in the fracture comparable to that found in the rock matrix is necessary, or reaction rates need to be at least slightly higher in the fracture. If secondary mineral precipitation rates are assumed to be 10 times greater in the fracture than in the matrix, then it is possible to obtain a very different system behavior in which the fracture seals before the rock matrix. One might rationalize this mechanism as being the result of a greater hydrologic accessibility of surface area available for mineral precipitation in the fracture than in the matrix. Or it may be that nucleation of secondary minerals is enhanced in the fracture, thus generating reactive surface area at a greater rate there than in the rock matrix (Steefel and Van Cappellen, 1990). The higher rates in the fracture

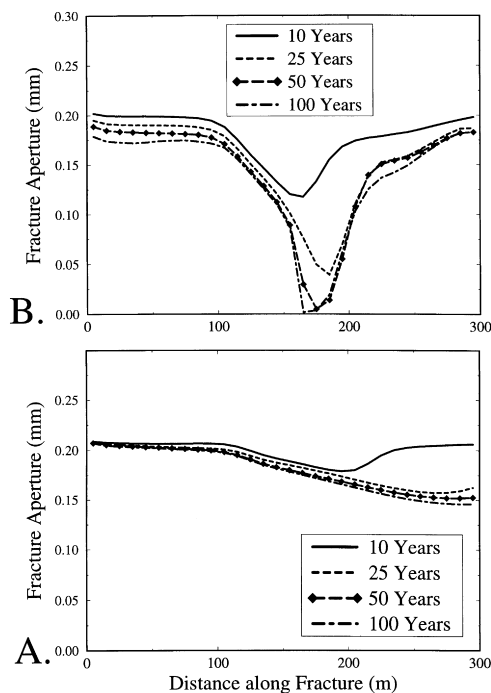


Fig. 10. Fracture aperture vs distance along fracture. (a) Case where reactive surface areas for secondary minerals in the rock matrix are equal to those in the fracture. (b) Case where reactive surface areas for secondary minerals in the rock matrix are 1/10 of the values in the fracture.

generate a gradient in concentration which drives a diffusive flux of reactive solutes into the fracture where they precipitate. The enhanced precipitation of secondary minerals in the fracture leads eventually to a reduction in fracture permeability [Fig. 10(b)] and a subsequent collapse of reaction zones upstream [Fig. 9(b)]. Initially, the gradual reduction in fracture permeability approximately balances the reduction in the porosity of the rock matrix (which reduces the effective diffusion coefficient), thus stabilizing the pH profile for up to about 50 years [Fig. 9(b)].

The two-dimensional behavior of the system is shown in Figs. 11 and 12. The simulations again assume values of the reactive surface areas of primary minerals to be 1/5 of the maximum values given in Table 4. They also assume a ratio of reactive surface area in the fracture vs the matrix of 10 to 1. In fracture–matrix systems without a feedback between reaction and the medium's porosity and permeability, relatively simple linear reaction front geometries

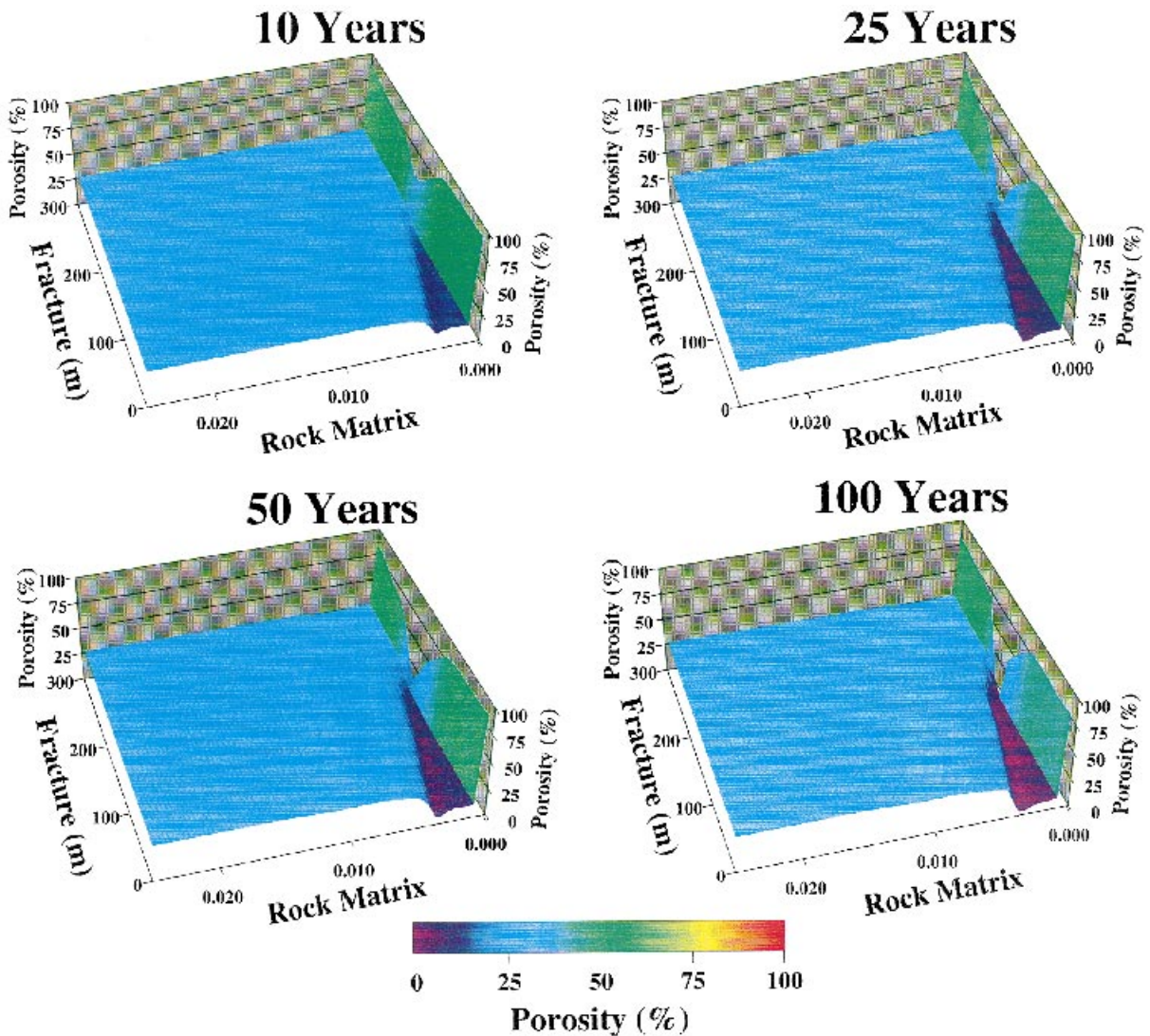


Fig. 11. Time evolution of the porosity in the fracture and rock matrix. This case assumes a reactive surface area for primary minerals 1/5 of the maximum value given in Table 4 and a ratio of reactive surface areas for secondary minerals in the fracture vs the matrix of 10–1.

develop (see Steefel and Lichtner, 1998 for an example). In contrast, the fully coupled system shows a more complex behavior in which the evolution of the porosity in the matrix and the fracture results in distortion of the front geometries. By 100 years, the porosity in the rock matrix approaches zero over a substantial distance along the fracture, while the fracture porosity approaches zero about 180 m from the fracture inlet. This decrease in porosity results in a reduction in fracture permeability, thus slowing the

rate of fluid flow, and a reduction in the effective diffusion rate in the rock matrix. The result is a limitation of the distance into the rock matrix and fracture that the high pH can migrate (compare early and late times in Fig. 12).

#### 7.5. Mineral paragenesis in the Maqarin fractures

The upstream collapse of reaction zones predicted by a model in which the fracture seals faster than the

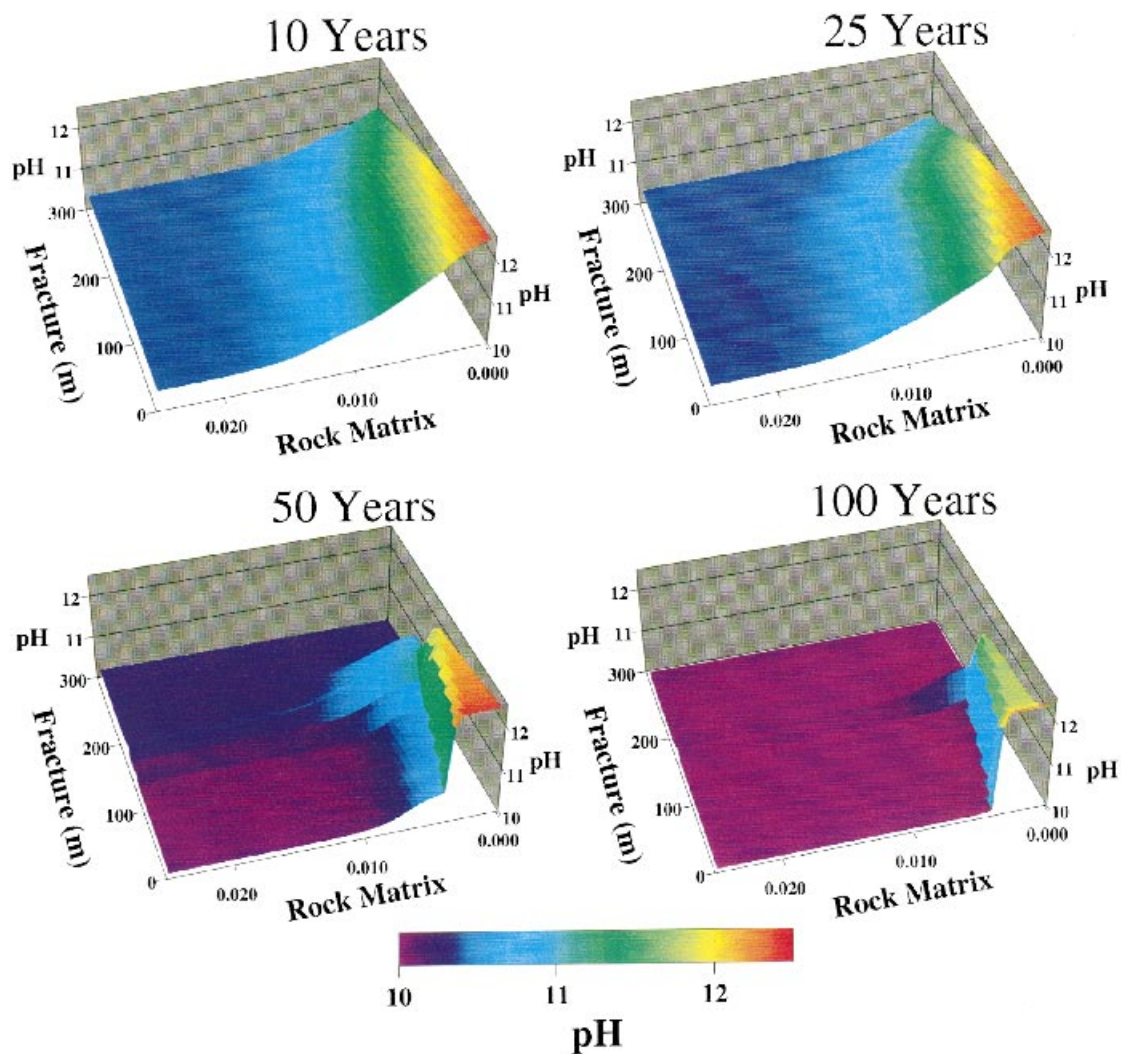


Fig. 12. Time evolution of the solution pH in the fracture and rock matrix. This case assumes a reactive surface area for primary minerals 1/5 of the maximum value given in Table 4 and a ratio of reactive surface areas for secondary minerals in the fracture vs the matrix of 10–1.

rock matrix results in a characteristic mineral paragenesis with time. Initially, ettringite is the dominant secondary mineral phase precipitating over a substantial portion of the fracture length. However, with the gradual sealing of the fracture and the resulting reduction in fracture flow velocity, mineral zones collapse upstream (Fig. 13). This causes a migration of the tobermorite (CSH) zone upstream over the ettringite zone. Such a time evolution results in a mineral paragenesis such as the one observed at 200 meters down the fracture and shown schematically in Fig. 14. This

represents at least part of the mineral paragenesis observed in the Eastern Spring occurrences at Maqarin (Alexander et al., 1998). Some of the previous modeling of the Maqarin hyperalkaline system (Smellie, 1998) has suggested that CSH phases develop closer to the fracture inlet than the ettringite does. We do find the CSH phase hillebrandite developing close to the fracture inlet, but in the simulations we have carried out, the bulk of CSH mineralization occurs downstream of the ettringite zone. Resolving the relative position of the CSH and ettringite zones is

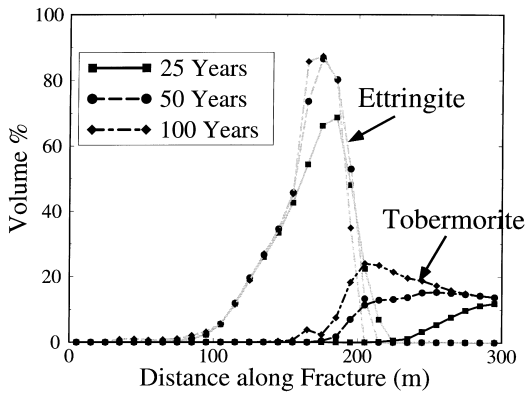


Fig. 13. Mineral volume fractions of the ettringite and tobermorite (CSH) in the fracture as a function of time. Note the upstream encroachment of tobermorite over ettringite.

clearly important, however, since it affects our interpretation of whether the mineral paragenesis observed in the Maqarin fractures indicates a downstream or upstream migration of reaction fronts. We argue here that gradual sealing of fractures may provide a single explanation for the mineral paragenesis observed in the field.

## 8. Discussion

The occurrences of hyperalkaline groundwater and alteration products at Maqarin Jordan provide a

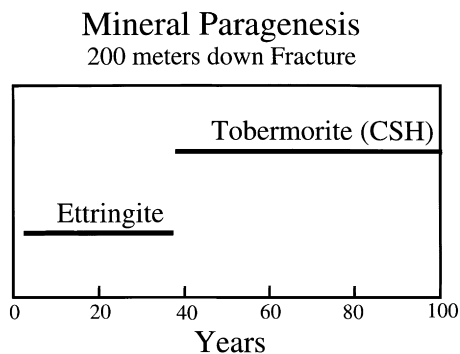


Fig. 14. Schematic representation of the mineral paragenesis at a distance of 200 m along the fracture based on time evolution shown in Fig. 13. Early formed ettringite is followed by the precipitation of CSH minerals. This paragenesis in the simulations is the result of the reduction in the permeability of the fracture which causes a collapse of the reaction fronts upstream.

possible natural analogue for low-level nuclear waste repositories constructed with significant amounts of cement. The Maqarin site is also particularly useful because much of the groundwater flow is along discrete fractures developed in otherwise relatively low permeability marl, much like that at the proposed Swiss low-level waste repository at Wellenberg. One of the critical questions concerning natural analogue sites, however, is their applicability to the nuclear waste repository in question. Clearly, if the analogue site is a perfect match for conditions at the repository site (this is extremely unlikely to be the case), then only minimal interpretation of the analogue site is necessary. If there are important differences, however, some level of interpretation is necessary in order to draw conclusions about the performance assessment of the nuclear waste repository based on observations at the analogue site. One possible way to maximize the usefulness of the analogue site is to carry out reactive transport modeling designed to capture the dynamics of the physical and geochemical system at the analogue site. To the extent that this ambitious goal is possible, it lays the basis for a rigorous analysis of the performance of a nuclear waste repository, even though conditions at the analogue site and waste repository are not identical. In addition, simulations of the natural analogue site may be useful in highlighting the fundamental sensitivities of the system. In other words, is it possible to obtain very different kinds of system behavior with relatively small changes in various parameters (e.g. reaction rate constants, initial porosities, etc.)? Although some might argue that this is a limitation on the usefulness of the modeling effort (since no single definitive answer can be provided), it may in fact be an essential result since it points out the unpredictable behavior of the natural system. This uncertainty must be taken into account in the design of a nuclear waste repository.

The simulations of the Maqarin system are at least partly successful at a number of levels. First, the modeling demonstrates that both the rock matrix alteration and the present-day groundwater compositions at the M1 and M2 sites in the A-6 adit can be interpreted in terms of reactive groundwater flow to the north-west along a set of discrete fractures. We have not established, however, that this is the only possible interpretation of the data. The modeling

predicts changes in solution chemistry and the formation of alteration products as a function of distance along the fracture which are compatible with the field observations. Analytical and numerical analyses indicate that the amount of reaction deduced from the change in rock matrix alteration width and solution pH are broadly comparable. This greatly enhances the usefulness of the Maqarin site, since it argues that the present-day system, as recorded in groundwater compositions (Waber et al., 1998), and the paleo-system as recorded in matrix and fracture secondary mineralization (Milodowski et al., 1998), may not be very different. Second, the modeling predicts many of the important secondary phases which are observed at Maqarin. Most important of these is the mineral ettringite (the dominant reaction product in all of the simulations carried out), followed by various CSH phases which occur in lesser amounts in both the fracture and the rock matrix.

After drawing these fundamental conclusions from the modeling study conducted here, more definitive statements become difficult to make because of the system sensitivity. Simulations carried out with equal reactive surface areas and rate constants in the fracture and matrix, for example, suggest that the rock matrix should seal first. In terms of the performance of a nuclear waste repository, this is a worst case scenario since it leads to a loss of the buffering capacity of the rock matrix (Steefel and Lichtner, 1994). The loss of the buffering capacity of the rock matrix due to its cementation leads to a downstream propagation of the hyperalkaline plume. However, field observations at Maqarin indicate that the fractures seal eventually, although some initial downstream propagation of fronts is not ruled out. The simulations indicate that one possible way to achieve this result is to have larger precipitation rates of secondary minerals in the fracture than in the matrix, presumably as a result of greater accessible reactive surface area in the fracture. With reactive surface areas only 10 times greater in the fracture than in the matrix, it is possible to seal the fracture and collapse the system upstream as a result of the permeability reduction. The sensitivity of the system indicated by these modeling results suggests that the behavior of a nuclear waste repository with a fractured near-field, and hyperalkaline groundwaters as a result of reaction with cement may not be easily predictable. Relatively small changes in a

system parameter like the reaction rate of secondary minerals can potentially lead to completely opposite behaviors. Moreover, the actual time scales for porosity and permeability reduction are also uncertain.

The simulations suggest that the mineral paragenesis observed in the Eastern Springs area of Maqarin might be interpreted as the result of sealing of fractures and the upstream collapse of reaction fronts. Most important of the observations is that ettringite dominates in the early stages of fracture mineralization while lesser amounts of CSH mineralization post-date ettringite.

It is clear that in order to draw much firmer conclusions from the Maqarin site, a more detailed knowledge of the fracture system is necessary. Particularly since the cubic law can not be expected to apply rigorously, it is essential to carry out both tracer tests and detailed field mapping and/or drilling of fractures to determine fracture apertures throughout the fracture system. In addition, field and/or laboratory tests of the reactivity of the rocks at Maqarin are necessary. Modeling of rock matrix alteration widths suggest that reactivities are high (close to experimentally-determined intrinsic reaction rate constants and maximum primary mineral surface areas). Presumably this could be confirmed by conducting flow or diffusion cell experiments involving both non-reactive and reactive fluids.

## 9. Conclusions

A numerical multicomponent reactive transport model fully described in Steefel and Lichtner (1998) was used to simulate the infiltration of hyperalkaline groundwater along discrete fractures at Maqarin, Jordan, a proposed natural analogue site to cement-bearing nuclear waste repositories. The simulations predicted that ettringite with lesser amounts of hillebrandite and tobermorite (hydrated calcium silicates or CSH phases) are the dominant alteration products formed at the expense of the primary silicates in the rock matrix and fracture, in qualitative agreement with observations at the Maqarin site. The simulations also predicted the pH of water samples collected along fractures at the M1 and M2 sites, with a fracture aperture of 0.22 mm giving the closest match with the data (within 13% of the value indicated by the rock matrix

alteration widths). The simulations suggested two possible scenarios for the time evolution of the fracture–rock matrix system. Where rate constants for secondary mineral precipitation reactions are the same in both the rock matrix and fracture, the rock matrix tends to become completely cemented before the fracture resulting in a downstream migration of the hyperalkaline plume. In contrast, if rates are as little as one order of magnitude higher in the fracture compared to the rock matrix (presumably due to a larger hydrologically accessible reactive surface area), it is possible to seal the fracture first, thus causing the mineral zones to collapse upstream as a result of the reduction in fracture permeability.

The sensitivity of the system indicated by these modeling results suggests that the behavior of a cementitious-based nuclear waste repository may not be easily predictable. Relatively small changes in a system parameter such as the rate constant or surface area of a secondary mineral can potentially lead to completely opposite behavior. Moreover, the actual time scales for porosity and permeability reduction obtained in the calculations are also uncertain. To clear up these uncertainties, experimental work is suggested involving flow or diffusion cell experiments for both non-reactive and reactive fluids. Further field work is also needed to constrain fracture apertures and velocities. The following references do not occur in the text: Aagaard and Helgeson, 1982; Alexander, 1992; Bear, 1979; Busenberg and Plummer, 1982; Dullien, 1979; Ge, 1997; Kirkner and Reeves, 1988; Lasaga, 1981; Lasaga, 1984; Lichtner, 1985; Lichtner, 1991; Lichtner, 1996; Norton and Knapp, 1977; Pedersen et al., 1998; Reed, 1982; Smellie, 1998; Yeh and Tripathi, 1989; Yeh and Tripathi, 1991.

### Acknowledgements

We are greatly indebted to Nick Waber of the Universität Bern for providing both data and helpful discussions of the Maqarin and hyperalkaline system. We also thank Nick, Carol Bruton, and Brett Leslie for their reviews of an early version of the manuscript, which spurred the present focus on the Maqarin system (whether they intended to do so or not). Careful reviews of the present version were provided by Nick Waber, Uli Mayer, Bill Murphy, and Kim Hunter. The

more recent financial support of the Nuclear Regulatory Commission in the US is also gratefully acknowledged. This report, however, does not necessarily reflect the views or regulatory position of the NRC.

### References

- Alexander W.R. (Ed.), 1992. A natural analogue study of cement-buffered, hyperalkaline groundwaters and their interaction with a sedimentary host rock. NAGRA Technical Report (NTB 91-10), Wetingen, Switzerland.
- Alexander W.R., Smellie, J.A.T., Milodowski A.E., Clark I., Hyslop E., Khoury H., Linklater C.M., Mazurek M., Salameh E., Waber H.N., 1998. Potential effects of hyperalkaline leachates on cementitious repository host rocks: an example from Maqarin, northern Jordan. *Geol. Soc. Engng Geol. Spec. Publ.* (in press).
- Cacas, M.C., Ledoux, E., de Marsily, G., Barbreau, A., Calmels, P., Gaillard, B., Margritta, R., 1991. Modelling fracture flow with a stochastic discrete fracture network: calibration and validation, 2. The transport model., *Water Resources Res.*, 26, 491–500.
- Caroll-Webb, S.A., Walther, J.V., 1988. A surface complexation model for the pH dependence of corundum and kaolinite dissolution rates. *Geochim. Cosmochim. Acta*, 52, 2609–2623.
- Chambers, A.V., Haworth, A., Ilett, D., Linklater, C.M., Tweed, C.J., 1998. Geochemical modeling: performance assessment issues. In: Smellie J.A.T. (ed.), 1998: Maqarin Natural Analogue Study: Phase III. SKB Technical Report TR 98-04, Stockholm, Sweden.
- Chou, L., Garrels, R.M., Wollast, R., 1989. Comparative study of the kinetics and mechanisms of dissolution of carbonate minerals, *Chem. Geol.*, 78, 269.
- Cvetkovic, V.D., 1991. Mass arrival of reactive solute in single fractures, *Water Resources Res.*, 27, 177–183.
- de Marsily, G., 1986. *Quantitative Hydrogeology*. Academic Press, New York, 440 p.
- Dove, P.M., 1995. Kinetic and thermodynamic controls on silica reactivity in weathering environments. In: White, A.F., Brantley, S.L. (Eds.), *Chemical Weathering Rates of Silicate Minerals*, *Reviews in Mineralogy*, vol. 31. Mineralogy Society of America, 1995, pp. 235–290.
- Drever, J.I., Clow, D.W., 1995. Weathering rates in catchments. In: White, A.F., Brantley, S.L. (Eds.), *Chemical Weathering Rates of Silicate Minerals*, *Reviews in Mineralogy*, vol. 31. Mineralogy Society of America, pp. 463–483.
- Dykhuizen, R.C., 1992. Diffusive matrix fracture coupling including the effects of flow channeling, *Water Resources Res.*, 28, 2447–2450.
- Khoury H.W., Salameh, E., Mazurek, M., Alexander, W.R., 1998. Geology and hydrogeology of the Maqarin area. In: Smellie J.A.T. (ed.), 1998: Maqarin Natural Analogue Study: Phase III. SKB Technical Report TR 98-04, Stockholm, Sweden.
- Knauss, K.G., Wolery, T.J., 1989. Muscovite dissolution kinetics as a function of pH and time at 70°C, *Geochim. Cosmochim. Acta*, 83, 1493–1502.

- Lichtner, P.C., 1988. The quasi-stationary state approximation to coupled mass transport and fluid–rock interaction in a porous medium, *Geochim. Cosmochim. Acta*, 52, 143–165.
- Maloszewski, P., Zuber, A., 1993. Tracer experiments in fractured rocks: matrix diffusion and the validity of models, *Water Resources Res.*, 29, 2723–2735.
- McKinley, I.G., Alexander, W.R., 1992. A review of the use of natural analogues to test performance assessment models of a cementitious near field, *Waste Man.*, 12, 253–259.
- McKinley, I., Alexander, W.R., 1993. Assessment of radionuclide retardation: uses and abuses of natural analogue studies, *J. Contam. Hydrol.*, 14, 249–261.
- Milodowski, A.E., Hyslop, E.K., Pearce, J.M., Wetton, P.D., Kemp, S.J., Longworth, G., Hodginson, E., and Hughes, C.R., 1998. Mineralogy and geochemistry of the western springs area. In: Smellie, J.A.T. (ed.), 1998: Maqarin Natural Analogue Study: Phase III. SKB Technical Report TR 98-04, Stockholm, Sweden.
- Moreno, L., Neretnieks, I., Eriksen, T., 1985. Analysis of some laboratory tracer runs in natural fissures, *Water Resources Res.*, 21, 951–958.
- Moreno, L., Neretnieks, I., 1993. Fluid flow and solute transport in a network of channels, *J. Contam. Hydrol.*, 14, 163–192.
- Moreno, L., Tsang, Y.W., Tsang, C.F., Hale, F.V., Neretnieks, I., 1988. Flow and tracer transport in a single fracture — a stochastic model and its relation to some field observations, *Water Resources Res.*, 24, 2033–2048.
- Moreno, L., Tsang, C.F., Tsang, Y.W., Neretnieks, I., 1990. Some anomalous features of flow and solute transport arising from fracture aperture variations, *Water Resources Res.*, 26, 2377–2391.
- Nagy, K.L., 1995. Dissolution and precipitation kinetics of sheet silicates. In White, A.F., Brantley, S.L. (Eds.), *Chemical Weathering Rates of Silicate Minerals*, Reviews in Mineralogy, vol. 31. Mineralogy Society of America, pp. 173–233.
- Neretnieks, I., 1980. Diffusion in the rock matrix: An important factor in radionuclide retardation? *J. Geophys. Res.*, 85, 4379–4397.
- Neretnieks, I., Eriksen, T., Tahtinen, P., 1982. Tracer movement in a single fissure in granitic rock: some experimental results and their interpretation, *Water Resources Res.*, 21, 849–858.
- Nordqvist, A.W., Tsang, Y.W., Tsang, C.F., Dverstorp, B., Andersson, J., 1996. Effects of high variance of fracture transmissivity on transport and sorption at different scales in a discrete model for fractured rocks, *J. Contam. Hydrol.*, 22, 39–66.
- Novak, C.F., 1996. Development of the FMT chemical transport simulator: coupling aqueous density and mineral volume fraction to phase compositions, *J. Contam. Hydrol.*, 21, 297–310.
- Novak, C.F., Sevougian, S.D., 1992. Propagation of dissolution–precipitation waves in porous media. In: Petruzzelli, D., Helfferich, F.G. (Eds.), *Migration and Fate of Pollutants in Soils and Subsoils NATO ASI Series. Series G: Ecological Sciences*, vol. 32. Springer, Berlin, pp. 275–307.
- Odling, N.E., Roden, J.E., 1997. Contaminant transport in fractured rocks with significant matrix permeability, using natural fracture geometries, *J. Contam. Hydrol.*, 27, 263–283.
- Park, C.K., Vandergraaf, T.T., Drew, D.J., Hahn, P.S., 1997. Analysis of the migration of nonsorbing tracers in a natural fracture in granite using a variable aperture channel model, *J. Contam. Hydrol.*, 26, 97–108.
- Parkhurst, D.L., 1995. User's guide to PHREEQC — a computer program for speciation, reaction-path, advective-transport, and inverse geochemical calculations. U.S. Geological Survey, Water Resources Investigations Report 95-4227.
- Phillips, O.M., 1991. *Flow and Reactions in Permeable Rocks*. Cambridge University Press, Cambridge, 285 p.
- Raven, K.G., Novakowski, K.S., Lapcevic, P.A., 1988. Interpretation of field tracer tests of a single fracture using a transient solute storage model, *Water Resources Res.*, 24, 2019–2032.
- Reardon, E.J., 1992. Problems and approaches to the prediction of the chemical composition in cement–water systems, *Waste Management*, 12, 221–239.
- Skagius, K., Neretnieks, I., 1986. Porosities and diffusivities of some nonsorbing species in crystalline rocks, *Water Resources Res.*, 22, 389–398.
- Smellie J.A.T., 1998, Executive summary. In: Smellie, J.A.T. (ed.), 1998: Maqarin Natural Analogue Study: Phase III. SKB Technical Report TR 98-04, Stockholm, Sweden.
- Smellie, J.A.T., Karlsson, F., Alexander, W.R., 1997. Natural analogue studies: present status and performance assessment implications, *J. Contam. Hydrol.*, 26, 3–18.
- Snow, D.T., 1968. Rock fracture spacings, openings, and porosities., *J. Soil Mech. Found. Div., Proc. Am. Soc. Civil Engrs*, 94, 73–91.
- Steefel, C.I., Lasaga, A.C., 1994. A coupled model for transport of multiple chemical species and kinetic precipitation/dissolution reactions with application to reactive flow in single phase hydrothermal systems, *Am. J. Sci.*, 294, 529–592.
- Steefel, C.I., Lichtner, P.C., 1994. Diffusion and reaction in a rock matrix bordering a hyperalkaline fluid-filled fracture, *Geochim. Cosmochim. Acta*, 58, 3595–3612.
- Steefel, C.I., Lichtner, P.C., 1998. Multicomponent reactive transport in discrete fractures, I. Controls on reaction front geometry. *J. Hydrol.*, 209, 186–199.
- Steefel, C.I., MacQuarrie, K.T., Approaches to modeling reactive transport in porous media. In: Lichtner, P.C., Steefel, C.I., Oelkers, E.H. (Eds.), *Reactive Transport in Porous Media*, Reviews in Mineralogy, vol. 34. Mineralogy Society of America, pp. 83–129.
- Steefel, C.I., Van Cappellen, P., 1990. A new kinetic approach to modeling water–rock interaction: the role of nucleation, precursors, and Ostwald ripening, *Geochim. Cosmochim. Acta*, 54, 2657–2677.
- Steefel, C.I., Yabusaki, S.B., 1996. OS3D/GIMRT, Software for Multicomponent–Multidimensional Reactive Transport, User Manual and Programmer's Guide, PNL-11166, Pacific Northwest National Laboratory, Richland, Washington.
- Tang, D.H., Frind, E.O., Sudicky, E.A., 1981. Contaminant transport in fractured porous media: analytical solution for a single fracture, *Water Resources Res.*, 17, 555–564.
- Therrien, R., Sudicky, E.A., 1996. Three-dimensional analysis of variably-saturated flow and solute transport in discretely-fractured porous media, *J. Contam. Hydrol.*, 23, 1–44.

- Thoma, S.G., Gallegos, D.P., Smith, D.M., 1992. Impact of fracture coatings on fracture/matrix flow interactions in unsaturated, porous media, *Water Resources Res.*, 28, 1357–1367.
- Tsang, Y.W., Tsang, C.F., 1989. Flow channeling in a single fracture as a two-dimensional strongly heterogeneous permeable medium, *Water Resources Res.*, 25, 1076–2080.
- Vandergraaf, T.T., Drew, D.J., Archambault, D., Ticknor, K.V., 1997. Transport of radionuclides in natural fractures: some aspects of laboratory migration experiments, *J. Contam. Hydrol.*, 26, 83–95.
- Waber H.N., Clark, I.D., Salameh, E., Savage, D., 1998. Hydrogeochemistry of the Maqarin area. In: Smellie J.A.T. (ed.), 1998: Maqarin Natural Analogue Study: Phase III. SKB Technical Report TR 98-04, Stockholm, Sweden.
- White, A.F., 1995. Chemical weathering rates of silica minerals in soils. In: White A.F., Brantley, S.L. (Eds.), *Chemical Weathering Rates of Silicate Minerals, Reviews in Mineralogy*, vol.31. Mineralogy Society of America, pp. 407–461.
- White, A.F., Brantley, S.L., 1995. Weathering rates of silicate minerals. In: White, A.F., Brantley, S.L. (Eds.), *Chemical Weathering Rates of Silicate Minerals, Reviews in Mineralogy*, vol. 31. Mineralogy Society of America, pp. 1–22.